UNIVERSITY OF TURIN

Master's Degree in Physics of Complex Systems

Master's Degree Thesis

Transients in Hippocampal Attractor Networks

Supervisors

Prof. Lamberto RONDONI

Prof. André LONGTIN

Candidate

Simone AZEGLIO

April 2021

Summary

The ability to process sequential information has always been considered as one of the most important features of biological and artificial intelligence systems. Although the investigation of learning and memory has a long history, little is known about possible dynamic principles of learning and remembering multiple events and their time sequence by neuronal systems. Here we propose a model based on results from the theory of nonlinear dynamics in neuroscience, in particular the concept of Winnerless Competition (WLC), which is an adequate candidate for sequential spatial memory. The essence of this idea is that sequential memory is encoded in a high-dimensional dynamical system which shows complex heteroclinic orbits that connect a sequence of saddle points. Each saddle point represents an event or pattern to be remembered. The existence and global stability of such a heteroclinic skeleton can be proven given the presence of asymmetric inhibitory connections. These connections are inevitably shaped by sensory inputs which sense the environment. In conclusion we will further support the plausibility of this model by showing its multifractality properties and how those can be connected to optimal search strategies.

Acknowledgements

During the writing of this thesis I received a lot of support and help.

First and foremost, I would like to thank my external supervisor, Prof. André Longtin, whose expertise in formulating research questions and methods has been invaluable. His insightful feedback has pushed me to think more sharply and take my work to the next level.

I would like to thank my colleagues from my Visiting Student Researcher position at the University of Ottawa for their excellent collaboration. In particular, I would like to single out my co-supervisor for the last two summers at the University of Ottawa, Prof. Leonard Maler. I would like to thank him for his patient support and for all the opportunities I was given to advance my research.

I would also like to thank my home supervisor , Prof. Lamberto Rondoni, for his invaluable guidance during my studies. He provided me with the tools I needed to choose the right direction and successfully complete my thesis.

In addition, I would like to thank my parents and family for their good advice and listening ear. Finally, I could not have completed this thesis without the support of Arianna, the entire MLJC group - and Prof. Caselle who have always believed in this project - , the RobLab team and my friends who often provided stimulating discussions as well as happy distractions to calm my mind outside of my research.

"In mathematical developments, the order in which the elements are placed is more important than the elements themselves"
Henry Poincaré

Table of Contents

List of Figures

Chapter 1

Spatial Navigation

Before we begin to illustrate our work, it is necessary to introduce some concepts that are radical to experimental testing in animal behavior. In the case of spatial navigation, we may identify several cognitive processes as important. First of all, navigation is not a pure process, but usually involves many different cognitive processes. These processes are both dynamic and multisensory, depending on the environment in which we move around. In the process of moving, we can consider various forms of information, which may lead to different strategies, and ultimately useful for finding a way to a specific destination. The input information is properly multisensory: visual, but also proprioceptive, somatosensory, vestibular and auditory. All of this information can - in combination or independently - help to extract information about the environment, the location of the target, and our own location. Navigation can also be seen as a dynamic process: when navigating, we obtain knowledge about the environment and store this information in memory so that it can be retrieved later for other purposes.

While observing animals moving, a physicist's perspective could primarily be the one of designing a *random-walk like* framework with the purpose of explaining the exploratory behaviour. It is indeed the case of *optimal search strategies*, which are going to be discussed in detail later on. This will be a qualitative and external point of view, which is very accurate in many cases. On the other hand, we can try to design a framework that involves internal representations of sensory stimuli, and learns to match these sensory inputs to a set of possible actions, possibly by generating behaviors that are in some way optimal for a specific exploratory task. Before entering the realm of dynamical systems and neuronal circuits, we will try to depict the experimental problem.

1.1 Animal Tracking

In neuroscience experiments quantifying behavioral traits is essential . Videography provides an easy way to observe and record animal behavior in different environments, but extracting specific aspects of behavior for further analysis can be very time-consuming, since there would be a significant amount of manual work. For example, in motion control trials, reflective markers on people or animals are used to help computer vision based tracking, with a few drawbacks: the markings are invasive, and the quantity and location of the markers has be determined a priori. Here, we will go through two different tools that can help experimenters in labelling animals' body parts. In the first case, *computer vision* techniques are used to handcraft features, while in the second case *deep learning* architectures are exploited to guarantee better accuracy and flexibility.

1.1.1 Fish Trajectories - Vistrack [1]

In our experiment, we consider a particular family of fish: Weakly Electric Fish (WEF). WEF species have the peculiarity of possessing a sort of sixth sense which allow them to sense their immediate (up to 3 centimenters) surroundings - even in the dark - through the generation of electric organ discharges (EODs). EODs time series can vary due to external conditions - sensory stimuli - or even self-movements. Given that the electric behavior of these fish can be perturbed by uncontrolled external sources which can generate different kinds of stimuli such as vibration, sound, electricity, and lights, it is of crucial importance to design a controlled environment through a very precise disposition of the experimental setup. Special precautions must be taken to block or attenuate external sensory stimuli during a long-term observation of free-swimming WEF (for an overview of the setup see [1]). In this way, changes in EOD rate and movement trajectories can be specifically attributed to stimuli presented by the experimenter.

The setup in [1] is suitable for video recording in the dark, through infrared cameras. After that, it is necessary to employ an animal tracking software, which can be either ready-to-use, e.g. Ethovision, or user-programmable through, for example MATLAB Image Processing Toolbox, In this case James Jun & colleagues developed a MATLAB library, named Vistrack (see Footnote 1 for the code). A video tracking software eventually needs a set of feature engineering operations which are specifically targeted to the problem of choice and requires trials and errors. At first, we need to perform a masking operation: a valid tracking area

[1] **Vistrack code, here on Github:** `https://github.com/jamesjun/vistrack`

needs to be defined by drawing a geometric shape to exclude the area outside. After this, an animal's shape needs to be isolated from the background by subtracting a background image from an image containing the animal. The subtracted image is converted into a binary format by applying an intensity threshold, such that the centroid and the orientation axis can be computed from binary morphological operations. In Gymnotiforms and Mormyrids, the species that we considered for this series of experiments, the electroreceptors are mainly concentrated in the head region. Thus the head position at any moment indicates a location of the highest sensory acuity. The head and tail locations can be automatically determined by applying the image rotation and bounding-box operations. The head and tail ends could be distinguished from one another by manually defining them in the first frame, and by keeping track of their locations from comparing two successive frames.

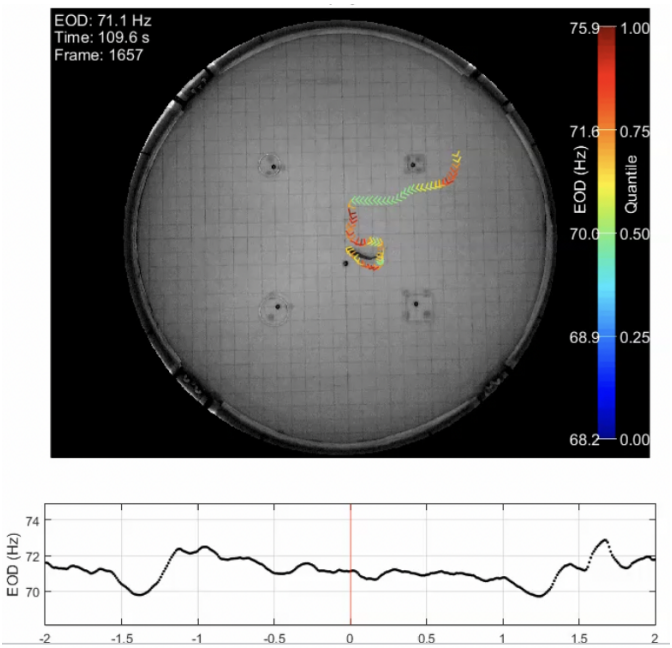

Figure 1.1: Vistrack tracking GUI

Employing the Vistrack library leads to concrete results for quantifying the learning process, in [2] more details are exhibited. For example, it is possible to distinguish between *early* and *late* trials: early trials represents exploratory strategy in a new and unknown environment, while late trials corresponds to trajectories traced by the fish after having learned where the target -food- is. Here we limit ourselves to some of these results, trajectory averaged statistics as in Figure 1.2 and trajectory reconstructions and density estimation as in Figure 1.3.

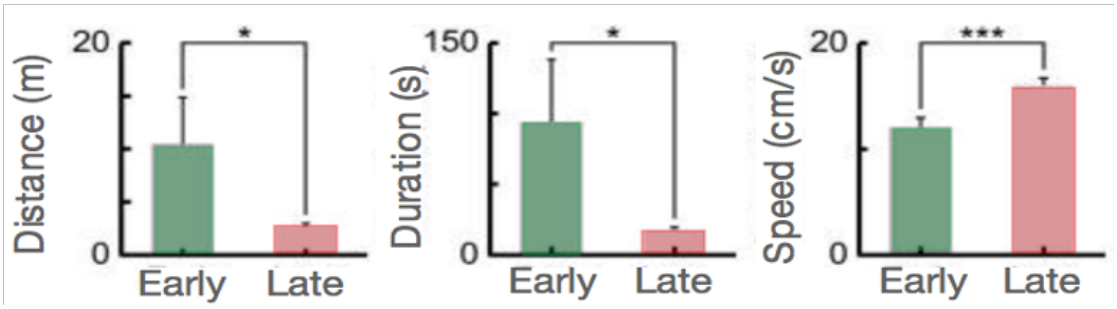

Figure 1.2: Learning process' metrics: *left* distance traveled from "home" to "target" by the fish in early vs late trials; *center* time spent from "home" to "target";*right* average speed in early vs late trials

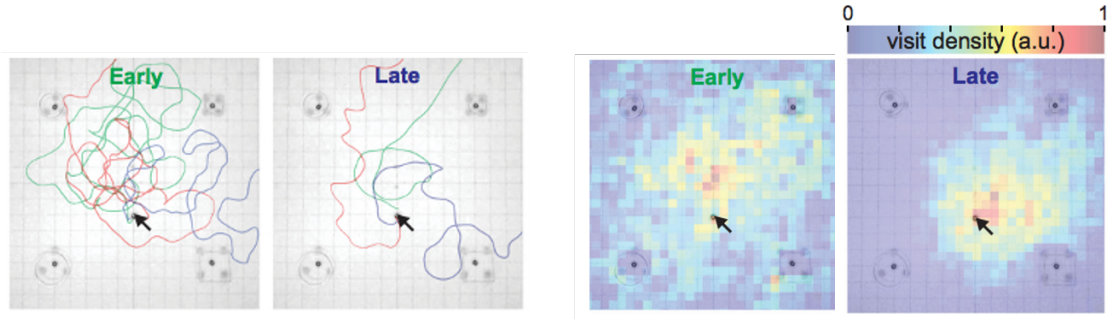

Figure 1.3: *Left* Trajectories of 3 different fish for early vs late trials;*right* Spatial density of trajectories averaged among different fish for early vs late trials

More details on the automated image tracking software are available in [1] and we will not go too deep into this part here. We decided to introduce the procedure in order to show how much feature engineering work there is by relying only on custom computer vision approaches. With the *deep learning revolution* in 2012 and the advent of GPUs, training deep neural networks in a reasonable time became feasible. This opened the door for the employement of such models into a plethora of real-world scenarios. In particular *Convolutional Neural Networks* (CNNs) have been succesfully brought into play in object detection problems, and luckily for us even in animal tracking, as we will see in the next subsection.

1.1.2 Mouse Trajectories - DeepLabCut [2]

Extracting the pose of animals can be made more efficient by employing Deep Learning architectures. One of the main problems of using such models is the fact that huge datasets - e.g. ImageNet [3]- are needed to let the deep neural network learn useful features, which is something hard to obtain for a neuroscience laboratory. In order to overcome this hurdle, Mackenzie Mathis' laboratory employed *transfer learning* techniques and designed a end-to-end model, DeepLabCut, for animal pose estimation [4]. In [4], they showed how it is possible to train a Convolutional Neural Network with only ~ 200 images, with human-like accuracy. One of the secrets for such a result is employing transfer learning: feature detectors of DeepLabCut are based on deep neural networks which are pretrained on ImageNet, de-facto learning low-level features from natural images statistics.

In order to get more precise labelling, we decided to employ DeepLabCut for a set of data involving mice moving inside a maze. Here we will illustrate some details of DeepLabCut's architecture which result in better accuracy and reduced manual labelling time with respect to Vistrack, which did not exploit machine learning techniques.

A quick overview of the most peculiar components of the model: feature detectors are variations of Deep Residual Networks (ResNet) [5], with readout layers which predict the position of body parts, while the key ingredient for semantic segmentation is the use of *deconvolutional layers* [6] (see Appendix for details).

The architecture in DeepLabCut is basically a variant of the original ResNet, already trained on ImageNet for the deeper layers but instead of keeping the readout layer at the output of the ResNet, they employed deconvolutional layers - i.e. transposed convolutional layer, to be more precise - to up-sample the convolved image and extract spatial probability densities for body parts. This probability density corresponds to the *evidence* of having a specific body-part in that place. To fine-tune the network for a particular task, its weights are trained on - manually - labeled data, which consist of frames and the accompanying annotated body part locations (see Figure 1.4).

The experiment we have considered is made up by a maze, with holes in the ground: a specific hole might contain food. In this case, the mouse orients itself by looking at the walls, which present different visual landmarks. The aim of this task is understanding whether the mouse has the ability of going from "home" -

[2] **DeepLabCut code here on Github:** `https://github.com/DeepLabCut/DeepLabCut`

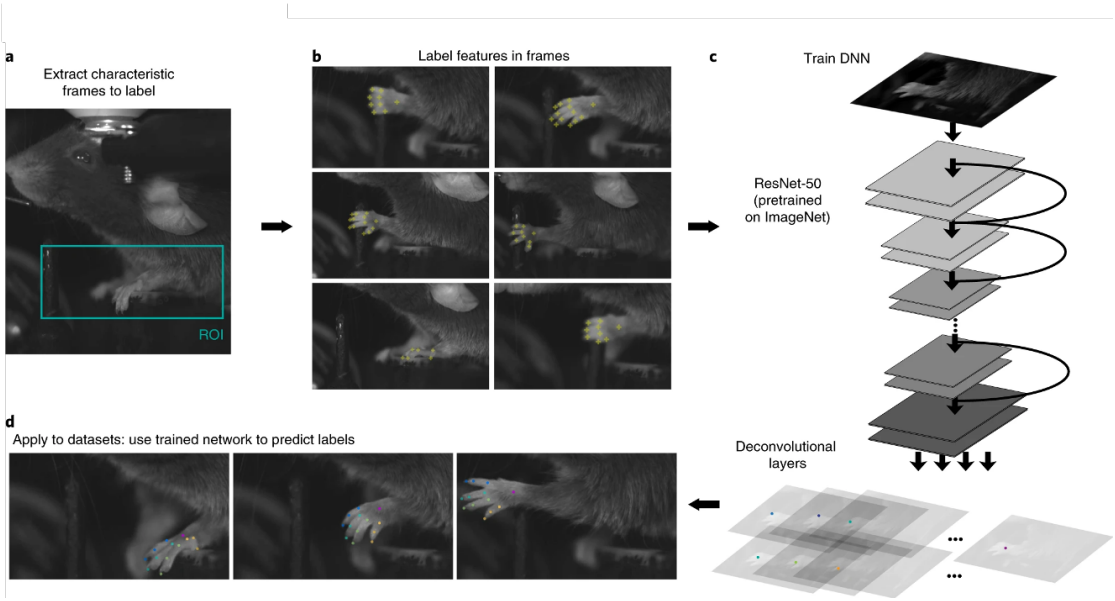

Figure 1.4: Deeplabcut procedure, taken from [4].

starting point - to "target" - where food is located, and improving the trajectory in terms of time spent, by exploiting spatial landmarks.

In our case, employing DeepLabCut, after minimal preprocessing - i.e. masking the maze - on considered videos (see Figure 1.5), significantly increased the accuracy (up to $\sim 98\%$) of labelling body parts as well as reduced the time taken to manually label many frames (significatly, $\sim 93\%$), with respect to Vistrack. Figure 1.6 shows an example trajectory, with four tracked body parts.

In this first section we presented our experiments, and, in particular how data in spatial navigation experiments look like. Building a model that explains this data is much less trivial than we might expect. This thesis will try to lay down a possible phenomenological model which is well grounded in nonlinear dynamics theory. But first of all, as a physicist would do, we will take a look at a possible way to explain spatial navigation in terms of optimal search strategies by unleashing statistical mechanics considerations.

1.2 Optimal Search Strategies

Every action we take is, in some way, the result of the invisible hand of evolution. In this terms, what would be the best statistical strategy to adopt in order to search for randomly located target sites? A forager - our agent - can show flight lengths with a characteristic scale, e.g. Gaussian, with well defined momenta. However

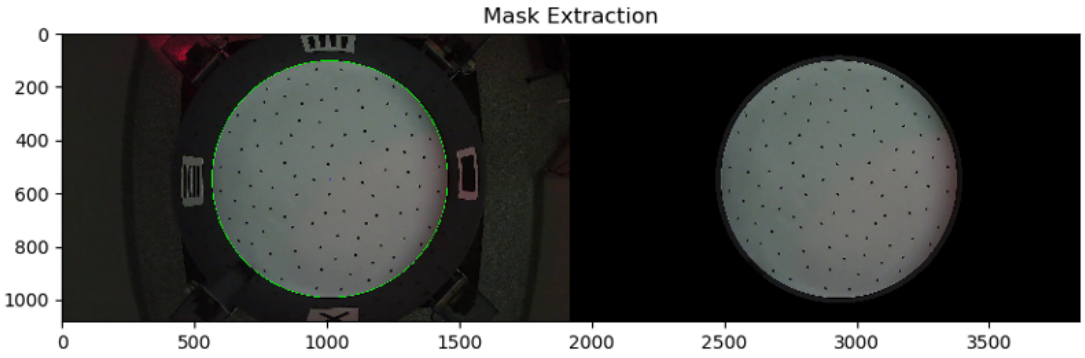

Figure 1.5: Preprocessing videos by imposing a mask around the maze. I have employed the OpenCV library in Python for these simple tasks.

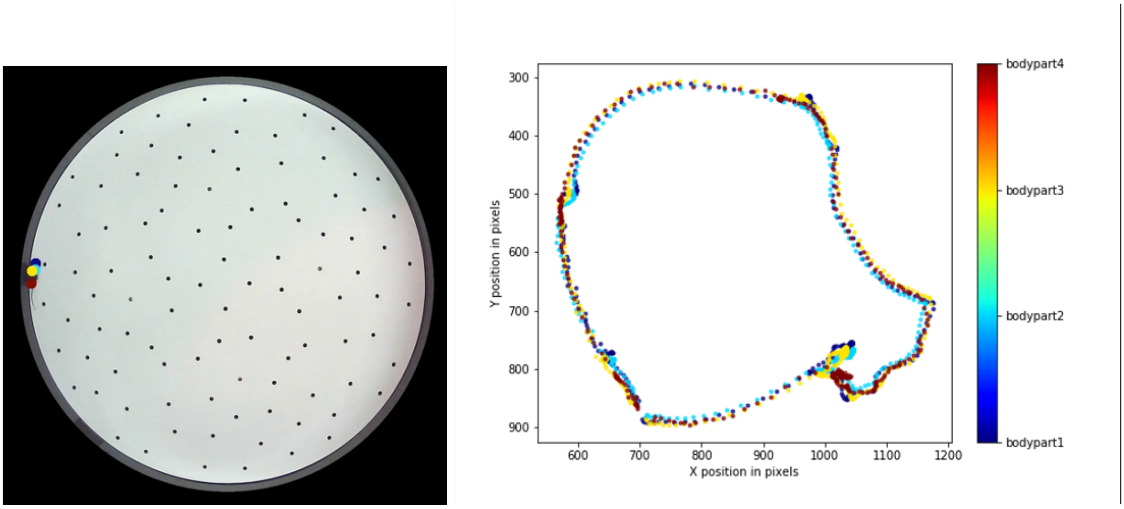

Figure 1.6: An example of trajectory with four tracked body parts. *Left* a frame of the original video, with mask applied; *right* tracked trajectory at the end of the video

in experiments which consider different animals, from albatrosses to fish, most of the time long-tailed power law distributions are observed for flight lengths and flight times [7] [8]. In our specific case, we consider an electric fish which moves around in a dark almost 2-D maze by exploiting its electric sense which can make it perceive its surrounding for ~ 3 cm away from its body surface - this is a result of evolution, since this fish' habitat mainly consists of muddy water its eyes would not be much effective. In [7], a model which can detects target sites only in its vicinity is proposed. More specifically, it is possible to study how the efficiency

of random searches depends on the underlying distribution. Levy flights can be shown to be the optimal strategy whenever target sites are sparse, random and non-destructive, i.e. they can be visited any number of times.

Levy flights have a characteristic distribution function with respect to flight length l_j:

$$P(l_j) \sim l_j^{-\mu} \tag{1.1}$$

where $1 < \mu \leq 3$. The central limit theorem states that for $\mu \geq 3$ we get a Gaussian distribution, while for $\mu \leq 1$ we get a probability distribution which cannot be normalized [9]. The approach will be to find the optimal value of parameter $\mu = \mu_{opt}$ for the search process. A Levy distribution is in general advantageous, whenever target sites are sparsely and randomly distributed, irrespective of the value of μ, because the probability to return to a previously visited site is smaller with respect to Gaussian distribution, i.e. with a fixed number of steps, comparing Gaussian random walks and Levy walks will show that, in the second case we explore more space (see Figure 1.7).

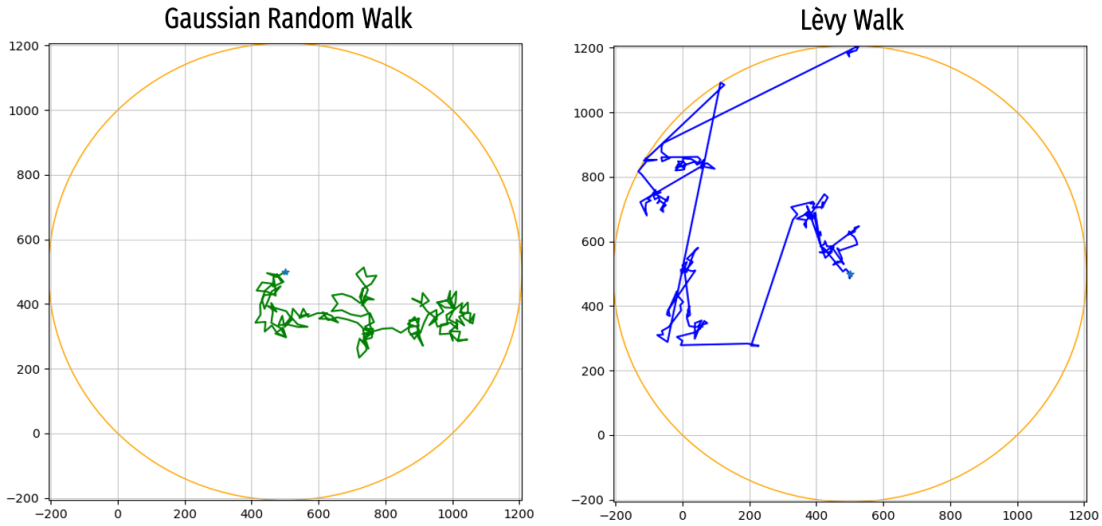

Figure 1.7: Python simulation for Gaussian Random Walks (*left*) vs Levy Walks (*right*), with the same $N_s = 1000$, i.e. number of steps.

It is possible to produce an idealized model where contributions due to learning processes are minimized, i.e. it corresponds to early trials of our fish experiment.

Moreover, we assume that our idealized animal moves as follows (see Figure 1.8):

- A *direct vision* distance r_v exists. If a target is closer than r_v the animal moves directly towards it. This is directly related to the fact that our fish can sense its environment within given physiological limits.
- In any other case, the animal selects a direction at random - i.e. from a uniform or Von Mises distribution - and samples a distance l_j from (1.1). After this it re-iterates the same procedure as long as it steps into a target.

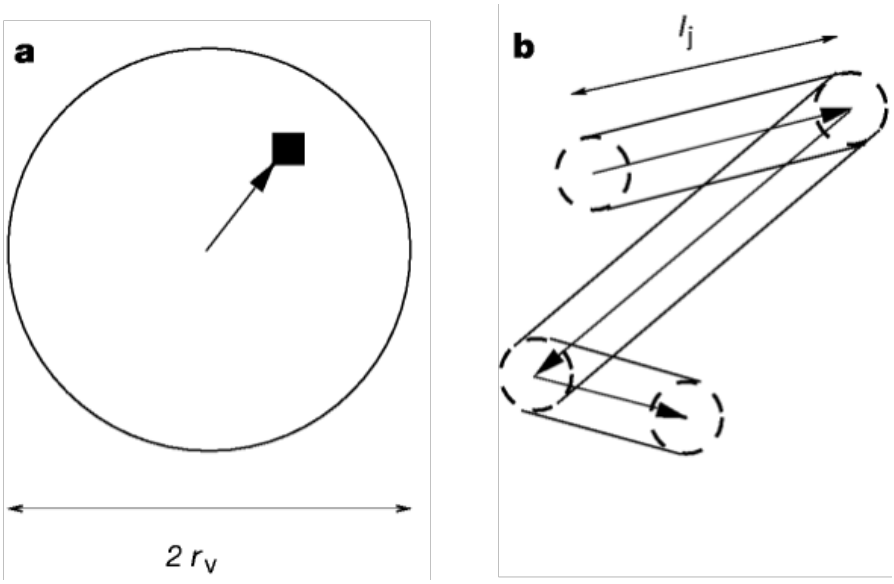

Figure 1.8: Foraging strategy as in [7]: (**a**); (**b**)

On the other side, the target site can be of two different types: *destructive* or *non-destructive*. In [7] they first solve the model analytically, by introducing the mean free path λ between successive targets - in a 2-D space, $\lambda \equiv (2r_v\rho)^{-1}$ where ρ is the target area density, i.e. density of food sources. We can calculate the mean flight distance as:

$$< l > \simeq \frac{\int_{r_v}^{\lambda} l^{1-\mu} dl + \lambda \int_{\lambda}^{\infty} l^{-\mu} dl}{\int_{r_v}^{\infty} l^{-\mu} dl} \tag{1.2}$$

$$= \left(\frac{\mu - 1}{2 - \mu}\right)\left(\frac{\lambda^{2-\mu} - r_v^{2-\mu}}{r_v^{1-\mu}}\right) + \frac{\lambda^{2-\mu}}{r_v^{1-\mu}} \tag{1.3}$$

which is an approximate calculation because we assumed that the distances between successive sites are all equal to λ. We also impose a finite cutoff λ on the probability distribution which leads to a truncated Levy distribution.

The effectiveness of a search strategy can be envisioned by defining the search efficiency function $\eta(\mu)$:

$$\eta = \frac{1}{N < l >} \tag{1.4}$$

where N is the average number of flight taken between successive targets. Finding a maximum of η will lead to the optimal value of μ. By considering the case of *destructive* foraging, the resultant mean number of flights N_d taken to travel an average distance of λ between two successive targets scales as - for $1 < \mu \leq 3$ - :

$$N_d \sim \left(\frac{\lambda}{r_v}\right)^{\mu-1} \tag{1.5}$$

In the case of Brownian motion we would have had: $N_d \sim (\lambda/r_v)^2$ - for $\mu \geq 3$. Let us consider the case of *non-destructive* foraging now. In this case, previously visited sites can be revisited so that the result that we have already found overestimates the mean number of flights N_n in the non-destructive case.

Let r_0 be the small distance between the last visited target site and the position after the first subsequent flight. For the non-destructive - Brownian walker - case $N_n = (\lambda - r_0)r_0/(2D)$, the scaling is not quadratic anymore, but linear, because the previous site, a small distance r_0 away, can be revisited. Indeed for $1 < \mu \leq 3$, it follows:

$$N_n \sim \left(\frac{\lambda}{r_v}\right)^{\frac{\mu-1}{2}} \tag{1.6}$$

In [7], the case in which target sites are sparsely distributed - $\lambda \gg r_v$ - is studied. By substituting (1.3) and (1.5) into (1.4), for non-destructive foraging the efficiency η has no maximum. On the other side, for non-destructive foraging if $\lambda \gg r_v$, then $N_d \gg N_n$, and by substituting into (1.4) and differentiating with respect to μ we

get a maximum for η at:

$$\mu_{opt} = 2 - \frac{1}{\ln^2(\lambda/r_v)} \tag{1.7}$$

This basically means that whenever is not possible to have a priori knowledge about the distribution of target sites, an optimal strategy for non-destructive foraging is to choose $\mu_{opt} = 2$ when $\lambda/r_v \gg 1$.

Furthermore, equations (1.5) and (1.6) describe the correct scaling properties even in the presence of short-range correlations in the directions and lengths of the flights. Short-range correlations can alter the variance of the distribution $P(l)$, but cannot change μ, so that this result remain valid. Hence, learning and short-term memory effects become unimportant in the long-time, long-distance limit. Last but not least, a finite λ ensures that the longest flights are not energetically impossible.

We have nestled the problem of spatial navigation into the framework of optimal search strategies, which is purely based on behavior and external characteristics of the system which processes this information, i.e. the brain. The aim of this thesis is to sketch a phenomenological model which takes into account neuronal dynamics, and specifically tries to connect the Levy walk exploration strategy to spiking neurons from first principles of nonlinear dynamical systems. In chapter 2 we introduce the main character of this tale, *inhibition*.

Chapter 2

Inhibitory Synapses

Our daily life is a sequence of multiple decisions. Should I continue after a M.Sc. and get a PhD or start working? Should I say "Hello" to the person I see on the other side of the street - in these days, it would presumably be the other side of the screen - or move on? Should I eat a slice of cake or an apple? Some are, of course, choices of minor relevance, but others could massively condition the course of our life.

Mathematically, decisions are more easily framed in the context of *games*. Here, we are going to borrow, implicitly, much of the terminology from *game theory*. We are going to contextualize the concept of competition and competitive dynamics, from a microscopic - single neuron - perspective. And we will try to understand how to scale it up, in order to make a suitable framework for decision making. The essence of this treatment lies in the concept of *inhibition*, where the actors are *inhibitory synapses*.

The role of inhibition is central in information processing tasks: it is the basis for the neural selection mechanism which decides whether a population of neurons is selected for engagement. Such a rule for selection implies some competition, generally speaking. The competitive behaviour of neuronal systems has been investigated in a plethora of works, starting from [10], [11]. We will show how inhibition effects shape this competition among neurons.

More specifically, we are going to explore the effects of *lateral inhibition* and *self-inhibition* on the membrane dynamics. A notable finding is that by combining the two, as we will show later on, we can extract a *control parameter* which basically governs two qualitatively different types of behavior. An equal strength of lateral and self-inhibition leads a network of neurons to the well-known *Winner-Takes-All* (WTA) behaviour. If, on the other side, the lateral inhibition is weaker with respect

to the self-inhibition, we will see the *Winners-Share-All* (WSA) behaviour: only a certain number of neurons - usually more than one - will be activated in the steady state.

2.1 Winner-Takes-All (WTA)

Here, by following the rate coding paradigm [12], we consider two *mutually inhibitory neurons* represented by their *firing rate*:

$$\begin{cases} \tau \dot{I}_1 = -I_1 + S(k_1 - \alpha I_2) \\ \tau \dot{I}_2 = -I_2 + S(k_2 - \alpha I_1) \end{cases} \tag{2.1}$$

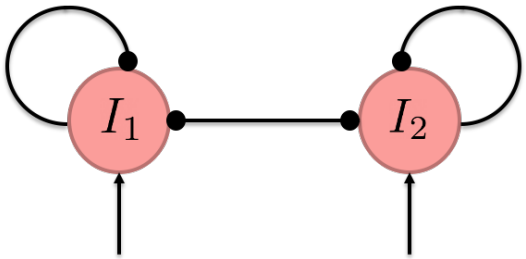

Figure 2.1: Representation of two mutually inhibitory neurons

where S can be any sigmoid function, in this case we consider, for example, the *Naka-Rushton* potential [13]

$$S(kx - \theta) = \begin{cases} \frac{M(kx-\theta)^2}{\sigma^2 + (kx-\theta)^2} & if \quad kx - \theta \geq 0 \\ 0 & if \quad kx - \theta < 0 \end{cases} \tag{2.2}$$

In this "network", one neuron will eventually prevail, de facto remaining the only one active. We also have an external stimulus k, which we take to be constant, for the sake of simplicity. Here α represents the weight of the inhibitory connection.

Thus, a specific value of I_1 will eventually *decide* whether I_2 is active or inactive and vice-versa. By inspecting, for example, $S(k_1 - \alpha I_2)$, if $I_2 > \frac{k_1}{\alpha}$ then $S(k_1 - \alpha I_2) = 0$, which leads to:

$$\begin{cases} \tau \dot{I}_1 = -I_1 \\ \tau \dot{I}_2 = -I_2 + S(k_2 - \alpha I_1) \end{cases} \tag{2.3}$$

At equilibrium we have $I_1^* = 0$ and $I_2^* = S(k_2)$, and vice-versa by switching subscripts. In fact, we can spot two stable fixed points:

$$\begin{cases} I_1^* = 0 \\ I_2^* = S(k_2) \end{cases} \qquad \begin{cases} I_1^* = S(k_1) \\ I_2^* = 0 \end{cases}$$

This is the essence of the *Winner-Takes-All* behaviour: only one neuron is active and *wins* the competition. For the symmetry of the system, there might exist an unstable fixed point, somewhere in the middle, which separates the basins of attraction.

By drawing the phase portrait as in Figure 2.2, we can have a visual confirmation of our intuition.

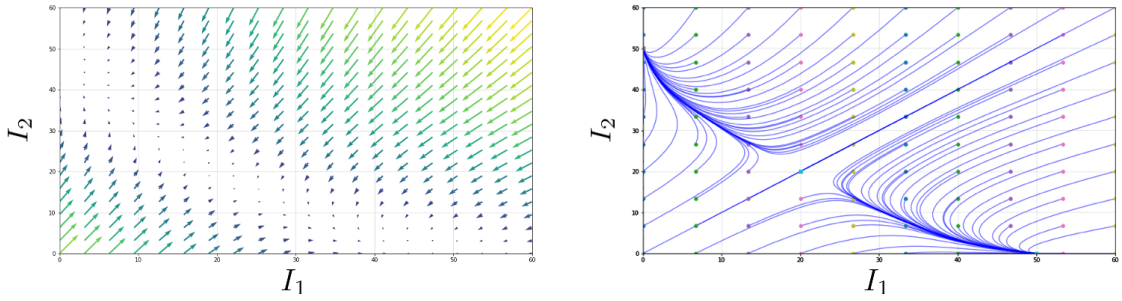

Figure 2.2: *Left:* quiver plot: phase space of the system for $M = 100$, $k_1 = k_2 = 120$, $\alpha_1 = \alpha_2 = 3$, $\sigma = 120$; *right:* phase portrait for different initial conditions, same value of parameters.

2.2 Competition in Neuronal Models

We have started this chapter by talking about the intimate relation between competition and neuronal dynamics: here we unveil a formal derivation, firstly investigated by *T. Fukai & S. Tanaka* in [14], which determines, in mathematical terms, the profound connection that we have previously anticipated.

Let's consider a system of N neurons, in which each of its elements is characterized by the following two equations:

$$\begin{cases} \tau \dot{u}_i(t) = -\lambda u_i(t) + I_i(t) \\ z_i = f(u_i - \theta) \end{cases} \tag{2.4}$$

where u_i represents the membrane potential, I_i the input current and z_i the

firing rate of the ith neuron, with $i = 1, ..., N$. Moreover, $I_i(t)$ can be decomposed into three different elements:

$$I_i(t) = \gamma + W_i - \sum_j V_{ij} z_j \tag{2.5}$$

where γ is a scalar value, representing the background activity, W_i is the neuron specific sensory stimulus and V_{ij} represents the strength of lateral inhibition connections: their role will be crystal clear while exploring the features of this system.

f is indeed a nonlinear function, usually a sigmoid, as we have anticipated in the previous subsection - i.e. the Naka-Rushton potential. In this case we assume f to be the logistic function:

$$f(x) = \frac{f_0}{1 + e^{-\beta x}} \tag{2.6}$$

where f_0 represents the maximum value, i.e. the maximum biological activity. Now, the dynamics of the firing rate would be:

$$\dot{z}_i = \frac{df(u_i(t) - \theta)}{dt} = -\frac{f_0(-\beta e^{-\beta(u_i - \theta)})}{(1 + e^{-\beta(u_i - \theta)})^2} \dot{u}_i$$

$$= \frac{\beta z_i e^{-\beta(u_i - \theta)}}{1 + e^{-\beta(u_i - \theta)}} (-\lambda u_i + I_i(t)) \tag{2.7}$$

Now, by considering (2.6), we can write :

$$e^{-\beta(u_i - \theta)} = \frac{f_0}{z_i} - 1$$

By substituting this expression into (2.7) we get:

$$\dot{z}_i = \frac{\beta z_i (f_0 - z_i)}{f_0} \Big(-\lambda\theta + \frac{\lambda}{\beta} \ln\Big(\frac{f_0 - z_i}{z_i}\Big) + I_i(t) \Big)$$

By expliciting $I_i(t)$:

$$\dot{z}_i = \frac{\beta z_i (f_0 - z_i)}{f_0} \Big(\gamma - \lambda\theta + \frac{\lambda}{\beta} \ln\Big(\frac{f_0 - z_i}{z_i}\Big) + W_i - \sum_j V_{ij} z_j \Big)$$

It follows that, if $z_i \ll f_0$, i.e. if the firing rate is always much smaller than the maximum value f_0, we have $\frac{f_0 - z_i}{z_i} \simeq 1$ and by rescaling as $\beta(\gamma - \lambda\theta)t \to t$, $\frac{W_i}{(\gamma - \lambda\theta)} \to W_i$ and $\frac{V_{ij}}{(\gamma - \lambda\theta)} \to V_{ij}$ we get:

$$\dot{z}_i = z_i\Big(1 + W_i - \sum_j V_{ij} z_j\Big) + \frac{\lambda}{\beta f_0(\gamma - \lambda\theta)} z_i(f_0 - z_i) \ln\Big(\frac{f_0 - z_i}{z_i}\Big) \tag{2.8}$$

The second term on the right-hand side indicates that the nonlinear output function has two asymptotes, i.e. positive values for $z_i \ll f_0$, negative values for $z_i \simeq f_0$. In biological jargon, this term preserves the boundedness of the membrane potential.

Given that we are considering a system with global inhibitory connections for which we are not getting close to f_0, we can ignore the negativity of that term and substitute it with a positive constant ϵ. This replacement doesn't change the qualitative behaviour of the considered dynamics.

In the end we obtain a *Lotka-Volterra* type equation:

$$\dot{z}_i = z_i\Big(1 + W_i - \sum_j V_{ij} z_j\Big) + \epsilon \tag{2.9}$$

What we have derived here is a quantitative link between neurons and competitive behavior: a *Lotka-Volterra* equation for firing activity from the standard equation for membrane dynamics.

2.3 Winners-Share-All (WSA)

Let's consider a N neurons system of the same kind as in (2.10), which has both *self-inhibition* and uniform *lateral inhibition* , so that matrix V is determined by:

$$V_{ii'} = \begin{cases} 1 & if \quad i = i' \\ k & if \quad i \neq i' \end{cases} \tag{2.10}$$

Here k represents the relative strength of the lateral inhibitory connections with respect to the self-inhibitory ones. For mathematical simplicity, we assume k to be

a constant, i.e. uniform lateral inhibition. This assumption take us from Eq. (2.9) to:

$$\dot{z}_i = z_i\Big(1 - z_i - k\sum_{j\neq i} z_j + W_i\Big) + \epsilon \tag{2.11}$$

Starting from Eq. (2.11) we will understand how k, as previously stated, can be seen as a *control parameter* for this system. To different values of k, the system in Eq (2.11) presents different behaviors. In particular, when $k \geq 1$ the network exhibits the WTA behavior, see for example [15].

There is another case, which shows intriguing properties, for $0 < k < 1$: namely, the *Winners-Share-All* (WSA) behavior. The peculiarity of this case is that the system admits more than one winner receiving inputs larger than some critical value determined by the distribution of intensity of the inputs. In order to show the direct link between inputs and this type of behavior, we will need to make a few assumptions:

- $\epsilon \geq 0$, $W_i > 0\ \forall i$
- ϵ satisfies $m\epsilon \ll W_i \quad \forall i \in M$, with $M = \{1, 2, ..., m\}$ being the *winner set* and m its cardinality, i.e. the number of winners.
- W_i's obey the following inequality with respect to their magnitudes:

$$W_1 \geq W_2 \geq W_3 \geq ... \geq W_{N-1} \geq W_N \geq 0$$

Firstly, let's set $\epsilon = 0$, while the case where $\epsilon \neq 0$ can be analyzed in a perturbative manner. Given $\epsilon = 0$ and $0 < k < 1$, we would like to look for stable fixed point solutions in Eq. (2.11), which yields to:

$$\begin{cases} \sum_{j\in M} K_{ij} z_j^{(M)} = 1 + W_i & if \quad i \in M \\ z_i^{(M)} = 0 & if \quad i \notin M \end{cases} \tag{2.12}$$

Where K is a $m \times m$ matrix:

$$K = \begin{pmatrix} 1 & k & . & . & k \\ k & 1 & & & . \\ . & & . & & . \\ . & & & . & k \\ k & . & . & k & 1 \end{pmatrix}$$

Since $k \neq 1$, K is not singular and thus invertible (K is a square matrix by definition):

$$K^{-1} = \frac{1}{(k-1)\alpha} \begin{pmatrix} k-\alpha & k & . & . & k \\ k & k-\alpha & & & . \\ . & & . & & . \\ . & & & . & k \\ k & . & . & k & k-\alpha \end{pmatrix}$$

where $\alpha = mk + 1 - k > 0$. Now that we have K^{-1}, we can solve the first Eq. in (2.12), we thus get:

$$z_i = \frac{mk-\alpha}{(k-1)\alpha} + \frac{(k-\alpha)W_i}{(k-1)\alpha} + \frac{(m-1)k}{(k-1)\alpha} \cdot \frac{1}{m} \sum_{j \neq i} W_j$$

which, by substituting $mk = \alpha + k - 1$, gives us:

$$z_i = \frac{1}{\alpha} + \frac{W_i}{1-k} + \frac{mk}{(k-1)\alpha} < W >_M \tag{2.13}$$

where $< W >_M = \frac{1}{m} \sum_j W_j$ is the average on the set of winners.
In this last equation, there is a key message, due to the second term on the right hand side: *the winners receiving larger inputs, acquire larger values of activity* z_i.

So far we have seen how competition between neurons, inhibitory synapses and sensory stimuli, can shape the activity of neuronal networks. In particular, we will continue to exploit the leitmotiv of competitive neurons in order to lay the foundations for a nonlinear dynamics principle which guarantees the existence of a well-defined structure in the phase space, which is ultimately essential for reproducing real-world behavior in neuronal networks. In the next chapter, we will talk about this principle, namely the Winnerless Competition principle and we will try to understand its effects on neuronal dynamics.

Chapter 3

Dynamical Principles

In the previous chapter, we have set the basis for building an information processing framework: *inhibition* is the key player. Starting from *inhibitory synapses*, we would like to establish a more grounded principle, based on nonlinear dynamics theory, namely: the *Winnerless Competition* (WLC) principle.

Before starting to define the WLC principle, we would like to establish a better context, in particular, we need to operate a significant shift: experimental neuroscience is usually based on the implicit assumption that neural mechanisms can be approximated by steady-state measurements of neuronal activity, which, indeed, is not the case most of the times. On the other side of the coin, a state in which no stable equilibrium is achieved, i.e. *transient*, might be envisioned as a suitable description of neuronal networks behavior.

From a theoretical neuroscience perspective, the picture of assuming that behavior can be modeled by steady-states corresponds to a specific information processing framework which is well embodied by the *Hopfield Network* [16], where attractors can be seen as minima of a energy function. We are not going to investigate this architecture in detail, but we are going to highlight in a better way the concept of "computing with attractors": given some input, a neural network will change its activation patterns, - i.e. active neurons - until it reaches an attractor state, i.e it settles into one pattern. It is important to underline a representative characteristic of this kind of systems, which is the fact that a specific input is associated with properties of the whole network in an individual attractor state.

At this point, we can summarise this first class of architectures by stating that the emphasis has to be on stable attractors, where memories are intended as their cognitive equivalents. There is another, less intuitive, idea that emphasizes the role of transient dynamics. Since neuronal phenomena usually operate and

change on short time scales, classical attractor states, e.g. fixed point or limit cycles, cannot be reached most of the time, e.g. due to input changes. There is experimental evidence [17], [18], [19] of the existence of deterministic dynamics that reach classical attractor states without waiting for a long time. Lastly, attractor dynamics do not express useful dynamics: they do not care about the path taken to reach an attractor, but only about the end point, given some specific initial conditions.

Transient dynamics, alternatively, can be the key to a new theoretical framework mostly because they have two main features. Firstly, even though they cannot be described by classical attractors, they are robust to noise and reliable for small variations of the initial conditions; in this way, the succession of states visited by the system is overall stable. Secondly, transients are input specific as shown in [20], [21], [22] for odor representations, which means that they contain information about what caused them. Transient dynamics with such properties are usually expressed by systems with a large number of degrees of freedom but they can be understood in the context of nonlinear dynamical systems.

In order to start our discussion, we inherited the previous picture of competitive dynamics as the foundation for constructing this framework. Since we previously showed that neuronal models can be eventually described by *Lotka-Volterra* type equations, we decided to introduce the WLC principle with an example: the *May-Leonard* system.

3.1 Competitive Lotka-Volterras

Competitive Lotka-Volterra equations are models of the population dynamics of species competing for some common resource. They are related to the Lotka-Volterra equations, also known as predator-prey equations, a pair of first-order nonlinear differential equations, commonly used to model the dynamics of systems in which two species interact. The populations evolve in time according to this pair of equations:

$$\begin{cases} \dot{x} = \alpha x - \beta xy \\ \dot{y} = \delta xy - \gamma y \end{cases} \tag{3.1}$$

where:

- x is the number of preys;

- y is the number of predators;
- $\alpha, \beta, \gamma, \delta$ are interaction terms (positive real parameters).

If in this set of equations, the intrinsic population dynamics is exponential - i.e. $x = \alpha x$, for the competition equations, on the other hand, the logistic equation is the basis. The logistic population model, in the ecology literature, takes the form:

$$\dot{x} = rx(1 - \frac{x}{K}) \tag{3.2}$$

where r is the growth rate and K the so called carrying capacity, i.e. the maximum population size that can be sustained in some specific environment.

This model can be further generalized to any number of species competing against each other. By using the matrix formalism we can write:

$$\dot{x_i} = r_i x_i (1 - \sum_{j=1}^{N} \alpha_{ij} x_j) \tag{3.3}$$

where we pulled the carrying capacity K_i term into the α_{ij} terms.

In the case where $N = 3$ (i.e. three competitors), the Lotka-Volterra equations in **1.1**, possess a special class of solutions. We anticipate here that this class of solutions can be placed into the WLC framework, which is further explored in [23]. Generally speaking, we refer to this specific model as the *May-Leonard* system of equations [24]:

$$\begin{cases} \dot{x} = x(1 - x - \alpha y - \beta z) \\ \dot{y} = y(1 - \beta x - y - \alpha z) \\ \dot{z} = z(1 - \alpha x - \beta y - z) \end{cases} \tag{3.4}$$

Specifically, we made some assumptions in order to reduce the number of parameters (i.e. *12* parameters) with respect to (3). **(i)** In particular we've firstly made the symmetry assumption that $r_1 = r_2 = r_3 = r$; **(ii)** secondly, with respect to the competition, we've assumed that population y affects x as z affects y as x affects z, so that $\alpha_{12} = \alpha_{23} = \alpha_{31} = \alpha$; **(iii)** similarly $\alpha_{21} = \alpha_{32} = \alpha_{13} = \beta$.

We decided to rescale each population so that we have $\alpha_{ii} = 1$ and also rescale t so that we get $r = 1$.

3.1.1 Steady States

For the sake of simplicity, we bring back (4) here:

$$\begin{cases} \dot{x} = x(1 - x - \alpha y - \beta z) \\ \dot{y} = y(1 - \beta x - y - \alpha z) \\ \dot{z} = z(1 - \alpha x - \beta y - z) \end{cases}$$

The possible equilibrium solutions are the following (we are expressing them as points in the 3-dimensional population space): the origin, (0,0,0) ; 3 single-population solutions of the form (1,0,0); 3 two-population solutions of the form $(1-\alpha, 1-\beta, 0)/(1-\alpha\beta)$ and the 3-species equilibrium (1,1,1)/$(1+\alpha+\beta)$.

Specifically, for $r_i > 0$ (in our case $r_i = 1$) the 3-species equilibrium is stable if and only if the eigenvalues of the following matrix:

$$\begin{pmatrix} 1 & \alpha & \beta \\ \beta & 1 & \alpha \\ \alpha & \beta & 1 \end{pmatrix}$$

have positive real parts. This matrix is, in fact, an example of a special matrix, the so called *circulant* matrix, which has some peculiar properties, e.g. a general formula for writing down its eigenvalues [25], so that we get:

$$\begin{aligned} &\lambda_1 = 1 + \alpha + \beta \\ &\lambda_{2,3} = 1 - (\alpha + \beta)/2 \pm i(\sqrt{3}/2)(\alpha - \beta) \end{aligned}$$

In order to get the results for fixed points coordinates we have investigated the linear stability of the May-Leonard system. Starting from:

$$\begin{cases} x(1 - x - \alpha y - \beta z) = 0 \\ y(1 - \beta x - y - \alpha z) = 0 \\ z(1 - \alpha x - \beta y - z) = 0 \end{cases} \tag{3.5}$$

we immediately identify (0,0,0) as a fixed point. So that we now have to consider
:

$$\begin{cases} 1 - x - \alpha y - \beta z = 0 \\ 1 - \beta x - y - \alpha z = 0 \\ 1 - \alpha x - \beta y - z = 0 \end{cases} \tag{3.6}$$

Let's look for the 3-species equilibrium (i.e. $x \neq 0, y \neq 0, z \neq 0$).

By substitution, starting from $x = 1 - \alpha y - \beta z$, we get for the second equation:

$$\begin{aligned} 0 &= 1 - \beta(1 - \alpha\mathbf{y} - \beta\mathbf{z}) - \mathbf{y} - \alpha\mathbf{z} \\ &= 1 - \beta + \alpha\beta\mathbf{y} + \beta^2\mathbf{z} - \mathbf{y} - \alpha\mathbf{z} \\ &= 1 - \beta + \mathbf{y}(\alpha\beta - 1) + \mathbf{z}(\beta^2 - \alpha) \end{aligned}$$

which leads to

$$\mathbf{y} = \frac{1 - \beta + (\beta^2 - \alpha)\mathbf{z}}{1 - \alpha\beta} \tag{3.7}$$

Now we have to backpropagate for getting $\mathbf{x}$, so that:

$$\begin{aligned} \mathbf{x} &= 1 - \alpha\left(\frac{1 - \beta + (\beta^2 - \alpha)\mathbf{z}}{1 - \alpha\beta}\right) \\ &= 1 - \frac{\alpha(1 - \beta)}{1 - \alpha\beta} - \left(\frac{\alpha(\beta^2 - \alpha)}{1 - \alpha\beta} + \beta\right)\mathbf{z} \end{aligned}$$

Now we can substitute into the third May-Leonard equation, to get:

$$\mathbf{z} = 1 - \alpha\left(1 - \frac{\alpha(1 - \beta)}{1 - \alpha\beta} - \left(\frac{\alpha(\beta^2 - \alpha)}{1 - \alpha\beta} + \beta\mathbf{z}\right)\right) - \beta\left(\frac{1 - \beta + (\beta^2 - \alpha)\mathbf{z}}{1 - \alpha\beta}\right)$$

By grouping z's coefficients:

$$\mathbf{z}\left(1-\alpha\left(\frac{\alpha(\beta^2-\alpha)}{1-\alpha\beta}+\beta\right)+\frac{\beta(\beta^2-\alpha)}{1-\alpha\beta}\right)=1-\alpha\left(1-\frac{\alpha(1-\beta)}{1-\alpha\beta}\right)-\frac{\beta(1-\beta)}{1-\alpha\beta}$$

$$\mathbf{z}\left(\frac{\alpha^3+\beta^3-3\alpha\beta+1}{1-\alpha\beta}\right)=\frac{1-\alpha\beta-\alpha(1-\alpha\beta)+\alpha^2(1-\beta)}{1-\alpha\beta}$$

Which leads to:

$$\mathbf{z}=\frac{\alpha^2+\beta^2-\alpha\beta-\alpha-\beta+1}{\alpha^3+\beta^3-3\alpha\beta+1} \tag{3.8}$$

It doesn't resemble mathematical beauty at all, let's try to simplify it. We can start by renaming:

$$\begin{aligned}\mathbf{N}&=\alpha^2+\beta^2-\alpha\beta-\alpha-\beta+1\\ \mathbf{D}&=\alpha^3+\beta^3-3\alpha\beta+1\end{aligned}$$

Let's tessellate:

$$\begin{aligned}\alpha\mathbf{N}&=\alpha^3+\alpha\beta^2-\alpha^2\beta-\alpha^2-\alpha\beta+\alpha\\ \beta\mathbf{N}&=\alpha^2\beta+\beta^3-\alpha\beta^2-\alpha\beta-\beta^2+\beta\end{aligned}$$

So that, by summing these two terms:

$$\alpha\mathbf{N}+\beta\mathbf{N}=\alpha^3+\beta^3-2\alpha\beta-\alpha^2-\beta^2+\alpha+\beta$$

Let's subtract it from $\mathbf{D}$ and see if we are far from finding a decomposition of our initial fraction:

$$\mathbf{D}-(\alpha\mathbf{N}+\beta\mathbf{N})=\alpha^2+\beta^2-\alpha\beta-\alpha-\beta+1$$

which is nothing but **N** itself, so that we have found:

$$\mathbf{D} = \mathbf{N}(\alpha + \beta + 1)$$

□

This finding finally leads to:

$$\mathbf{z} = \frac{1}{\alpha + \beta + 1} \tag{3.9}$$

In the end, by substituting back, the complete solution is:

$$\begin{cases} \mathbf{x} = \frac{1}{\alpha+\beta+1} \\ \mathbf{y} = \frac{1}{\alpha+\beta+1} \\ \mathbf{z} = \frac{1}{\alpha+\beta+1} \end{cases} \tag{3.10}$$

There are 6 more solutions, 3 single population and 3 two-population solutions. To verify their existence, we can just set one or two variables to 0, in mathematical terms calculations are more trivial with respect to the 3-species fixed point and we get the previously mentioned results.

3.1.2 Linear Stability

Now it's time to compute the Jacobian matrix, **A**:

$$A_{i,j} = \frac{\partial F_i}{\partial x_j} = \begin{pmatrix} 1 - 2\mathbf{x} - \alpha\mathbf{y} - \beta\mathbf{z} & -\alpha\mathbf{x} & -\beta\mathbf{x} \\ -\beta\mathbf{y} & 1 - \beta\mathbf{x} - 2\mathbf{y} - \alpha\mathbf{z} & -\alpha\mathbf{y} \\ -\alpha\mathbf{z} & -\beta\mathbf{z} & 1 - \alpha\mathbf{x} - \beta\mathbf{y} - 2\mathbf{z} \end{pmatrix} \tag{3.11}$$

By having the Jacobian matrix, we can inspect the linear stability of the previously found fixed points, by solving $det(\mathbf{A} - \lambda\mathbf{I})$, where **I** denotes the identity matrix and *det*, the determinant. By substituting the fixed points coordinates we get:

- For (**x**, **y**, **z**) = (0,0,0), we get $\lambda_{1,2,3} = 1 > 0$ thus an unstable point, as expected;

- For $(\mathbf{x}, \mathbf{y}, \mathbf{z}) = (1,0,0)$, we get $\lambda_1 = -1, \lambda_2 = 1-\beta, \lambda_3 = 1-\alpha$, which depends on both α and β (for WLC to work it has to be a saddle point, see below) it works similarly for (0,1,0) and (0,0,1);
- For $(\mathbf{x}, \mathbf{y}, \mathbf{z}) = (1-\alpha, 1-\beta, 0)/(1-\alpha\beta)$, we get

$$\lambda_1 = \frac{\alpha^2 + \beta^2 - \alpha\beta - \alpha - \beta + 1}{1 - \alpha\beta}$$
$$\lambda_2 = \frac{\alpha + \beta - 2 - \sqrt{\alpha^2 + 4\alpha\beta^3 - 8\alpha\beta^2 + 2\alpha\beta + \beta^2}}{1 - \alpha\beta}$$
$$\lambda_3 = \frac{\alpha + \beta - 2 + \sqrt{\alpha^2 + 4\alpha\beta^3 - 8\alpha\beta^2 + 2\alpha\beta + \beta^2}}{1 - \alpha\beta}$$

  again, similar results for the other two (two-species) points.

- For $(\mathbf{x}, \mathbf{y}, \mathbf{z}) = (1,1,1)/(1+\alpha+\beta))$, we get (see symbolic solver in Python)

$$\lambda_1 = -1$$
$$\lambda_2 = \frac{\alpha - \sqrt{3}i\alpha + \beta + \sqrt{3}i\beta - 2}{2\alpha + 2\beta + 2}$$
$$\lambda_3 = \frac{\alpha + \sqrt{3}i\alpha + \beta - \sqrt{3}i\beta - 2}{2\alpha + 2\beta + 2}$$

In order to introduce the WLC principle, we are specifically interested in this last case, where every population is still alive, i.e. every neuron is active. The stability depends on the value of α and β. Let us select them to be $0 < \alpha < 1 < \beta$, the motivation will be explained in detail in the next section. With these values for α and β we are basically constraining the system to possess three different saddle-points, which can be noted in the phase portrait of the system, i.e. the right-side of Figure 3.1. Such a phase portrait corresponds to a sequential switching among the activities of the three neurons, i.e. left-side of Figure 3.1: a behaviour which embodies the essence of the competitive dynamics.

3.2 Winnerless Competition Principle

In the previous section, we had a quick glance at what are the key qualitative characteristics of the *Winnerless Competition Principle*. Here we are going to provide a more detailed and quantitatively grounded, in nonlinear dynamics theory, description. Before starting though, it is worth underlining explicitly the main point of this principle, which is basically the transformation of incoming *spatial inputs*

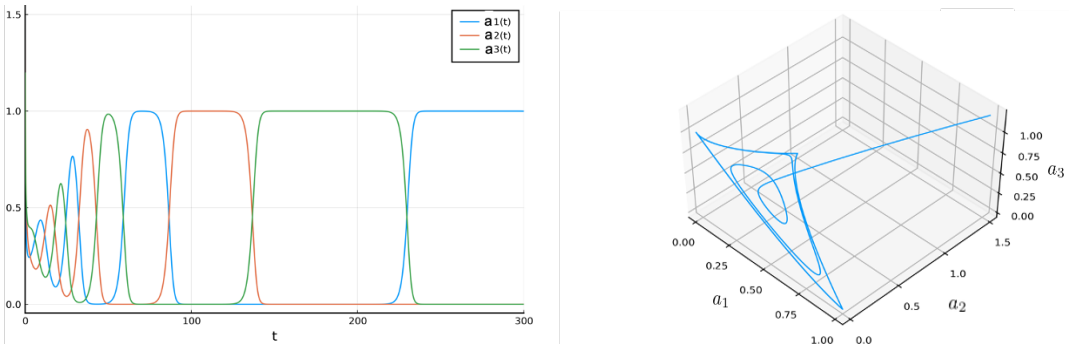

Figure 3.1: *Left:* Activity of each population (i.e. in our framework, each neuron); *right:* phase portrait for the May-Leonard system. Inspired by [24], [23], simulations have been carried out in Julia, see code).

into *temporal output* based on the intrinsic switching dynamics of the neuronal system. In the presence of sensorial stimuli, the sequence of the switching solely depends on the incoming information. In particular, there is a fundamental question that we are going to discuss below: how the WLC can be stable and what are the conditions for such a robustness?

For the sake of clarity, let us bring back the *May-Leonard* system's associated matrix:

$$\begin{pmatrix} 1 & \alpha & \beta \\ \beta & 1 & \alpha \\ \alpha & \beta & 1 \end{pmatrix}$$

We have briefly mentioned that the stability of the system, in the case where each population is alive, i.e. each neuron is active, depends on the values of α and β. More generally, having $\alpha \neq \beta$, corresponds to a special case of *nonsymmetric inhibition*. In fact, a detailed analysis is only possible for the case $N = 3$, as explained in [26], [27] and [28]. When $0 < \alpha < 1 < \beta$, a peculiar structure, in the phase space, exists, namely a *heteroclinic contour*, Figure 3.1 (right), that consists of saddle points and a one-dimensional separatrices connecting them. It can be proven that, in some regions of the phase space, such heteroclinic contour is a global attractor. The most interesting property, as showed in [28] is that if α and β depend on the sensory stimulus, i.e. a result of a learning procedure, the system can generate different heteroclinic contours for different input stimuli.

Here we are interested in understanding whether a heteroclinic contour exist and when it is stable. Heteroclinic contours are the geometrical image of the WLC

behavior. As we will show, these orbits exist only in the nonsymmetric inhibition case, when saddle points satisfy several conditions.

3.2.1 Existence and Stability of the Heteroclinic Contour

For the following treatment (see [23]) we consider the canonical *Lotka-Volterra* model:

$$\dot{a}_i = a_i\left[1 - \left(a_i + \sum_{i\neq j}^{N} \rho_{ij} a_j\right)\right] \tag{3.12}$$

A heteroclinic contour consists of a certain number of saddle equilibria, connected by finitely many heteroclinic orbits.

We can indicate by A_1 the following equilibrium point (1,0,0, ...,0), by A_2 the point (0,1, ...,0) and by A_N the point (0,0, ...,1). For the sake of simplicity, we are going to assume that there exist a heteroclinic orbit $\Gamma_{i,i+1}$ connecting the points A_i with A_{i+1}, $i = 1, ..., N$ and with $A_{N+1} \equiv A_1$. The heteroclinic contour can serve as an attracting set if every point A_i has only one unstable direction. A_i satisfies this assumption if $\rho_{ki} > 1$, where $k \neq i + 1$ and $\rho_{i+1,i} < 1$.

Now we can define the concept of *intersection of hyperplanes*:

$$P_{2i} = \bigcap_{j=1, j\neq i, i+1}^{N} \{a_j = 0\} \tag{3.13}$$

which is a two-dimensional invariant manifold containing A_i and A_{i+1} in such a way that A_i is a saddle point on P_{2i} and A_{i+1} is a stable node on P_{2i}. The system (3.12) on P_{2i} has the form: a

$$\dot{a}_i = a_i[1 - (a_i + \rho_{ii+1} a_{i+1})] \tag{3.14}$$

$$\dot{a}_{i+1} = a_{i+1}[1 - (a_{i+1} + \rho_{i+1i} a_i)] \tag{3.15}$$

And, from the previous assumptions, we have $\rho_{ii+1} > 1$ and $\rho_{i+1i} < 1$. This fact implies that there are no equilibrium points in the region where $a_i > 0$, $a_{i+1} > 0$ and since $\dot{a}_{i+1} < 0$ if $\rho_{i+1i} \gg 1$ then we certainly have a heteroclinic connection between

A_i and A_{i+1} on the plane P_{2i}. The specific case of $N = 3$ has been explicitly proven in [25].

The point A_i on P_{2i} is a stable node with *Lyapunov Exponents* $\lambda_1 = -1$ and $\lambda_2 = 1 - \rho_{ii+1}$. By observing Lyapunov exponents, we can determine the leading direction at A_{i+1}, in particular if $\lambda_1 > \lambda_2$ then the leading direction is parallel to the a_{i+1}-axis; while, on the other side, if $\lambda_1 < \lambda_2$ then the leading direction is transversal to the a_{i+1}-axis on P_{2i}. By assuming that the last inequality holds, we get $\rho_{ii+1} < 2$ which states that the majority of orbits go to A_{i+1} by following a direction $\mathbf{l} = (1, -\rho_{i+1i}/(2 - \rho_{ii+1}))$ transversal to the a_{i+1}-axis.

We can proceed by noting that the vector $\mathbf{l}$ on P_{2i} can be embedded into a hyperplane, namely $H_i : \{a_{i+2} = 0\}$ as $\mathbf{L} = (0,0,...,1,-\rho_{i+1i}/(2 - \rho_{ii+1}), 0, ..., 0)$ with 1 on the i_{th} place. Now, we would like to understand whether the direction $\mathbf{L}$ is the leading direction for the node A_{i+1} on hyperplane H_i.

Sufficient conditions for this assumption can be extracted by noting that Lypanunov exponents at point A_{i+1} of the system of equations (3.12) restricted to H_i are $1 - \rho_{ii+1}, ...,1 - \rho_{i-1i+1}, -1, 1 - \rho_{i+2i+1}, ..., 1 - \rho_{Ni+1}$, which are all negative given previous constraints on ρ. In case $\rho_{ki+1} > \rho_{ii+1}$ for $k \neq i$, then $1 - \rho_{ii+1}$ is the Lyapunov exponent closest to zero and $\mathbf{L}$ is the leading direction at A_{i+1} on H_i. We are going to assume that $\rho_{ki+1} > \rho_{ii+1}$ is satisfied even though this is not a necessary condition for the validity of the next result, but it certainly makes calculations easier.

It is time to exploit some results achieved in [29]: in particular it is possible to write down, by recalling that A_i is a saddle point on P_{2i}, a map from a transversal to the stable separatrix into a transversal to the unstable separatrix along the orbits going through a neighborhood of A_i. We can define a 2-D coordinate system (ξ, η) such that:

$$\xi = c\eta^{\nu_i} \tag{3.16}$$

where η is the deviation from the stable manifold, ξ is the deviation from the unstable one and c is a constant. On the other side, ν_i is the so-called *saddle value* [29], and is defined as:

$$\nu_i = -\frac{1 - \rho_{ii+1}}{1 - \rho_{i+1i}} \equiv \frac{\rho_{ii+1} - 1}{1 - \rho_{i+1i}} \tag{3.17}$$

The saddle value has a fundamental importance: if $\nu_i > 1$, the map (3.16) is a local contraction and A_i is a dissipative saddle; else, if $\nu_i < 1$, (3.16) is a local expansion.

Starting from the definition of saddle value, we can show how the contour $\Gamma = \bigcup_{i=1}^{N} \Gamma_i \cup A_i$ can be an attractor.

Theorem 1.[23] Assume that, as previously mentioned, $\rho_{ki} > 1$ with $k \neq i+1$, $\rho_{i+1i} < 1$, $\rho_{ii+1} < 2$ and $\rho_{ki+1} > \rho_{ii+1}$ with $k \neq i$ are satisfied and:

$$\nu = \prod_{i=1}^{N} \frac{\rho_{ii+1} - 1}{1 - \rho_{i+1i}} > 1 \tag{3.18}$$

(recall that $i+1 = 1$ if $i = N$). Then there is a neighborhood U of the contour Γ such that for any initial condition $a^0 = (a_1^0, ..., a_N^0)$ in U with $a_i^0 > 0$, one has $dist(a(t), \Gamma) \to 0$ as $t \to \infty$, where $a(t)$ is the orbit which passes by a^0.

Proof of Theorem 1. As shown in [23], the proof is based on constructing the *Poincaré map* along orbits in a neighborhood of the contour Γ. Consider the stable (unstable) manifold W_i^s (W_i^u) of the point A_i and P_i (Q_i) as a point of the heteroclinic orbit Γ_{i-1} (Γ_i) in a neighborhood of A_i.

Let S_{P_i} (S_{Q_i}) be a "portion" of a hyperplane, transversal to Γ_{i-1} (Γ_i) going through P_i (Q_i). In this way, a local map $f_i : S_{P_i} \to S_{Q_i}$ along orbits in a neighborhood of A_i is well defined. A proper coordinate system [29] becomes:

$$\xi_i = c_i \eta_i^{\nu_i}, \quad \chi_i = \varphi_i(y_i, \eta_i) \tag{3.19}$$

where $\eta_i \in \mathbb{R}$ is a coordinate on S_{P_i} parallel to W_i^u, $y \in \mathbb{R}^{N-2}$is a vector, transversal to the η_i-axis on S_{P_i}, ξ_i is a coordinate on S_{Q_i}, parallel to the leading direction on W_i^S at A_i, with the conditions:

$$\left|\frac{\partial \varphi_i}{\partial y_i}\right| \leq \bar{c}_i \eta_i^{\beta_i}, \quad \left|\frac{\partial \varphi_i}{\partial \eta_i}\right| \leq \bar{c}_i |y_i| |\eta_i|^{\beta_i - 1} \tag{3.20}$$

where $\bar{c}_i > 0$ is a constant and $\beta_i > \nu_i$.

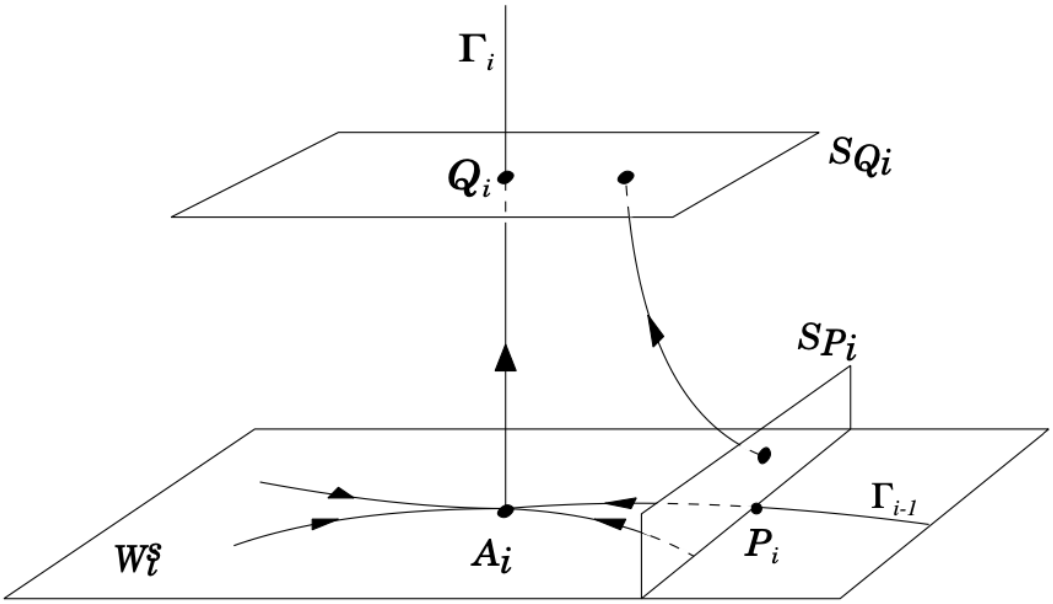

Figure 3.2: Local Map in the neighborhood of a saddle point (taken from [23])

Given that the heteroclinic orbit Γ_i joins point Q_i and P_{i+1}, the global map $F_i : \tilde{S}_{Q_i} \to S_{P_{i+1}}$ along orbits, is well defined where $\tilde{S}_{Q_i} \subset S_{Q_i}$ is a small neighborhood of the point Q_i on S_{Q_i}. This map is a diffeomorphism and has the form:

$$\begin{cases} \eta_{i+1} = a_{i1}\xi_i + a_{i2}\xi_i + o(\xi_i^2) \\ y_{i+1} = b_{i0} + b_{i1}\xi_i + b_{i2}\xi_i + o(\xi_i^2) \end{cases} \tag{3.21}$$

We should specify that the orbit Γ_i belongs to the intersection of invariant hyperplanes $\{a_j = 0\}, j \neq i, j \neq i+1$. Given that the hyperplane $\{\xi_i = 0\}$ on S_{Q_i} is mapped by F_i into the hyperplane $\{\eta_{i+1} = 0\}$ on $S_{P_{i+1}}$, this means that in (3.22), $a_{i2} = 0$ and $a_{i1} \neq 0$. This leads (3.22) to :

$$\begin{cases} \eta_{i+1} = a_{i1}\xi_i + o(\xi_i^2) \\ y_{i+1} = b_{i0} + b_{i1}\xi_i + b_{i2}\xi_i + o(\xi_i^2) \end{cases} \tag{3.22}$$

Now we have all the ingredients to construct a *Poincaré map* $F = S_{P_1} \to S_{P_1}$ as the superposition of maps f_i, F_i, i.e. basically $F = F_N \cdot f_N \cdot \cdots \cdot F_2 \cdot f_2 \cdot F_1 \cdot f_1$. The

map $F_i \circ f_i$ has the following form:

$$\begin{cases} \eta_{i+1} = a_{i1} c_i \eta_i^{\nu_i} + o(\eta_i^2) \\ y_{i+1} = b_{i0} + b_{i1} c_i \eta_i^{\nu_i} + b_{i2} \varphi_i(y_i, \eta_i) + ... \end{cases} \tag{3.23}$$

In the first order approximation, F along η-coordinates is independent of y-coordinates. We can consider the 1-D approximation:

$$\begin{cases} \eta_{i+1} = a_{i1} c_i \eta_i^{\nu_i} \quad i = 1, ..., N \\ \eta_{N+1} := \bar{\eta}_1 \equiv \tilde{F}(\eta_1) \end{cases} \tag{3.24}$$

Provided that (3.18) is satisfied, we can see that map $\tilde{F} : \eta_1 \to \bar{\eta}_1$ is a contraction. It follows that $\bar{\eta}_1 = C\eta_1^{\nu}$, where C is a constant. We can see how if $\nu > 1$, then $\partial\bar{\eta}_1/\partial\eta_1 < 1$ if η_1 is small enough, $\tilde{F}$ is a contraction and $\eta_1 = 0$ is an attracting fixed point.

Consider now the differential of $F_i \circ f_i$:

$$DF_i \circ f_i = \begin{pmatrix} a_i c_i \nu_i \eta_i^{\nu_i - 1} + ... & 0 + ... \\ b_{i1} c_i \nu_i \eta_i^{\nu_i - 1} + b_{i2} \frac{\partial \varphi_i}{\partial \eta_i} + ... & \frac{\partial \varphi_i}{\partial y_i} + ... \end{pmatrix} \tag{3.25}$$

because of this result (3.20):

$$||DF_i \circ f_i|| \leq B_i \eta_i^{\nu_i - 1} \tag{3.26}$$

where B_i is a constant. This last inequality leads to:

$$||DF \circ f|| \leq B \prod_{i=1}^{N} \eta_i^{\nu_i - 1} \tag{3.27}$$

with $B = \prod_{i=1}^{N} B_i$. We will estimate $\prod_{i=1}^{N} \eta_i^{\nu_i - 1}$ by using (3.23):

$$\prod_{i=1}^{N} \eta_i^{\nu_i - 1} = \eta_N^{\nu_N - 1} \cdot \eta_{N-1}^{\nu_{N-1} - 1} \cdot \cdots \cdot \eta_2^{\nu_2 - 1} \cdot \eta_1^{\nu_1 - 1}$$

Let us consider first $\eta_2^{\nu_2 - 1} \cdot \eta_1^{\nu_1 - 1}$, given that $\eta_2 = a_1 c_1 \eta_1^{\nu_1} + ...$, then:

$$\eta_2^{\nu_2-1} \cdot \eta_1^{\nu_1-1} = (a_1 c_1)^{\nu_2-1} \cdot (\eta_1^{\nu_1} + ...)^{(\nu_2-1)} \cdot \eta_1^{\nu_1-1} \leq const \cdot \eta_1^{\nu_1\nu_2-1}$$

Now, we can frame an inductive reasoning, so that for:

$$\begin{aligned}
\eta_3^{\nu_3-1} \cdot \eta_2^{\nu_2-1} \cdot \eta_1^{\nu_1-1} &= (a_2 c_2)^{\nu_3-1} \cdot (\eta_2^{\nu_2} + ...)^{\nu_3-1} \cdot \eta_1^{\nu_1-1} \\
&\leq const \cdot \eta_2^{\nu_3\nu_2-1} \cdot \eta_1^{\nu_1-1} \\
&= const \cdot (a_1 c_1)^{\nu_3\nu_2-1} \cdot (\eta_1^{\nu_1} + ...)^{\nu_3\nu_2-1} \cdot \eta_1^{\nu_1-1} \\
&\leq const \cdot \eta_1^{\nu_3\nu_2\nu_1-1}
\end{aligned}$$

For the *k-th* step:

$$\begin{aligned}
\eta_k^{\nu_k-1} \cdot \cdots \eta_2^{\nu_2-1} \cdot \eta_1^{\nu_1-1} &\leq const \cdot (a_1 c_1 \eta_1^{\nu_1} + ...)^{\nu_k \ldots \nu_2-1} \cdot \eta_1^{\nu_1-1} \\
&\leq const \cdot \eta_1^{\prod_{i=1}^{N} \nu_i - 1}
\end{aligned}$$

Therefore we have:

$$\prod_{i=1}^{N} \eta_i^{\nu_i-1} \leq C \cdot \eta_1^{\nu-1} \tag{3.28}$$

where C is constant. Finally we get:

$$||DF|| \leq BC\eta_1^{\nu-1} \tag{3.29}$$

which finally leads to our result: F is a contraction in a neighborhood of the point $(\eta_1 = 0, y_1 = 0)$, which corresponds to the contour Γ.

□

3.2.2 Birth of a Stable Limit Cycle

What happens if we impose a perturbation on our system?
Here we discuss about a direct corollary of **Theorem 1** which point out the

possibility of the birth of a stable limit cycle in system (3.12) when it is perturbed in an appropriate way. Technically, such a perturbation should promote the existence of an absorbing region and a fixed point inside the Poincaré map. We can start from (3.12) and add a small perturbation:

$$\dot{a_i} = a_i\left[1 - \left(a_i + \sum_{i\neq j}^{N} \rho_{ij}a_j\right)\right] + \epsilon\Psi_i(a) \tag{3.30}$$

where $\Psi_i(a)$ is a smooth function. For small $\epsilon > 0$, the system shows saddle equilibrium points $A_{i\epsilon}$ and separatrices $\Gamma_{i\epsilon}$.

Theorem 2.[23] Assume that conditions of **Theorem 1** are satisfied,

$$lt_{\epsilon\to 0}\left(\bigcup_{i=1}^{N}\Gamma_{i\epsilon}\right) = \Gamma \tag{3.31}$$

where *lt* means *topological limit*. Assume also that at least one of the separatrices $\Gamma_{i\epsilon}$ is not a heteroclinic orbit. Then for sufficiently small $\epsilon > 0$ the system (3.30) has a stable limit cycle L_ϵ in a neighborhood of Γ such that $lt_{\epsilon\to 0}L_\epsilon = \Gamma$.

The proof of **Theorem 2** can be done by constructing the Poincaré map, in a similar fashion to the proof of **Theorem 1**. Condition (3.31) is both necessary and sufficient for the existence of an absorbing region. The proof is done by employing the so-called *Annulus Principle* as in ([27], [30], [29]), and we are going to omit it here. One last consideration on the robustness of the system: the attractor of a perturbed system (3.30) is located in a small neighborhood of the *unperturbed* attractor.

In [23], numerical results for a six dimensional system ($i = 1, ...,6$) show how the limit cycle in the vicinity of the former heteroclinic contour is a global attractor, as in Figure 3.3. The system considered in [23] is of the following form:

$$\dot{a_i} = a_i\left[1 - \left(a_i + \sum_{i\neq j}^{N=6} \rho_{ij}a_j\right)\right] + \epsilon a_i a_{i+3} \tag{3.32}$$

where $i + 3 \equiv i - 3$ if $i > 3$, with $\epsilon = 0.01$. The connection matrix on the other side is of the form:

$$\rho = \begin{pmatrix} 1 & 0 & 5 & 0 & 0 & 1.5 \\ 1.5 & 1 & 0 & 2 & 0 & 0 \\ 0 & 1.5 & 1 & 0 & 5 & 0 \\ 0 & 0 & 1.5 & 1 & 0 & 2 \\ 5 & 0 & 0 & 1.5 & 1 & 0 \\ 0 & 2 & 0 & 0 & 1.5 & 1 \end{pmatrix}$$

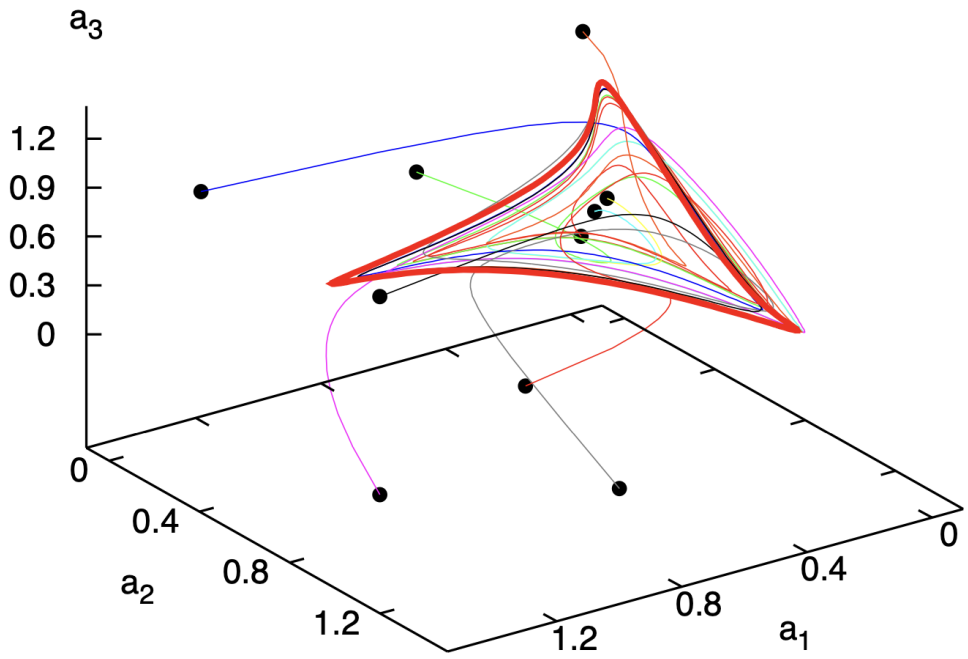

Figure 3.3: 3D projection of the 6-dimensional system (taken from [23])

3.2.3 On the Capacity of WLC Networks

As we have previously stated, when the inhibitory connections are not symmetric, i.e. $\rho_{ij} \neq \rho_{ji}$, the system possesses heteroclinic orbits which consist of saddle points and 1-dimensional separatrices connecting them. From **Theorem 1**, we know that such heteroclinic orbits are indeed global attractors in phase space. The idea is that, by slightly changing the sensory stimulus - i.e. the input - , another orbit in the vicinity of the previous heteroclinic one becomes a global attractor. It is possible to quantify the capacity C of such a network (as in [28]), which basically tells the number of different memories the network could encode.

In order to estimate C, we assume that at least one heteroclinic orbit exist. It is fairly simple to understand how from one heteroclinic orbit, we can build many other from it by permuting the indices of a_i and of the matrix ρ: there are $N!$ permutations of the indices. Some of these permutations generate the same heteroclinic orbit, e.g. with $N = 6$ as in the previous example: (1,2,3,4,5,6) and (2,3,4,5,6,1) are equivalent. This leads to N cyclically equivalent permutations out of a given permutation. Thus, the number of heteroclinic orbits involving all N neurons is $(N-1)!$, but we should note that there exist more heteroclinic orbits, i.e. the ones associated with the $N-1$, $N-2$ ... 3 dimensional subspaces which can be selected by "deleting" one saddle point at a time. The total number of these possible heteroclinic orbits is the capacity C:

$$C = \sum_{k=3}^{N} \binom{N}{k} (k-1)! = N! \sum_{k=3}^{N} \frac{1}{k(N-k)!} \tag{3.33}$$

We also know that:

$$\frac{N!}{3} \sum_{k=0}^{N-3} \frac{1}{k!} < C < \frac{N!}{N} \sum_{k=0}^{N-3} \frac{1}{k!}$$

for large N, we get:

$$\left(1 - \frac{1}{e(N-2)!}\right) < \frac{C}{e(N-1)!} < \frac{N}{3}\left(1 - \frac{1}{e(N-2)!}\right) \tag{3.34}$$

which in the end leads to $C \approx e(N-1)!$.

Chapter 4

Biological Plausibility

In principle, it should be possible to observe reproducible transient behavior in any complex network with nonsymmetric connections. In this chapter we consider one canonical model, namely the *Hodgkin-Huxley* (HH) spiking model. As we show both rigorously and with computational models, a network made of HH neurons exploits a Stable Heteroclinic Contour (SHC) in its phase space. One of the main drawbacks of the HH neuron model is its computational complexity: even though it is one of the most biologically plausible models, each HH neuron is described by four equations. Furthermore by considering synapse dynamics in order to build a network, the number of equations lifts up to six. What we are going to do is to show that a HH neuron network can be reduced in terms of complexity by noting that a neuronal rate model is equivalent with respect to bifurcations and phase portrait. We demonstrate how to pull out this reduced rate model; its form is significantly similar to the Fukai & Tanaka model, with minor differences. In this way, we observe how competitive dynamics are embodied in the nature of neuronal networks.

4.1 Hodgkin-Huxley Neuronal Model

In their paper in 1952 [31], Alan Hodgkin and Andrew Huxley described a model with the aim of explaining the mechanism underlying the initiation and propagation of action potentials in the squid giant axon. A few years later, in the 1963, they received the *Nobel prize in Physiology or Medicine* for this work.

Given the relevance of this work and the fact that we are going to use this model to establish the validity of a Lotka-Volterra-like reduced model which presents WLC behavior, we decided to briefly present it here, mainly from a physicist's perspective. In this view, a neuron is basically an element that when excited with

a sufficient amount of current, emits an action potential - or spike - i.e. a sharp electrical potential across its cell membrane. Luckily, the neuronal cell membrane can be modelled as an electric circuit (as in Figure 4.1), so that we can transpose the problem into a physically sound one.

Hodgkin and Huxley distinguished among different types of ion currents [31] while performing experiments on the giant axon: *sodium*, *potassium* and a *leak* current, mainly composed by *chloride* ions. The flow of those ions is controlled by specific voltage-dependent ion channels for sodium and potassium, while the leak current takes into account other channel types which are not described explicitly.

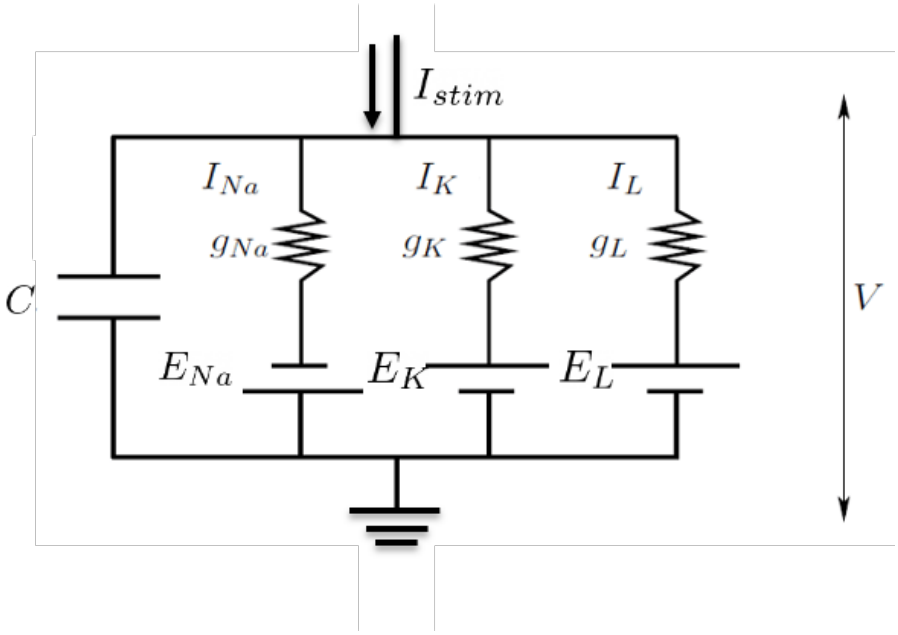

Figure 4.1: A HH neuron can be modelled as a circuit

In this picture, the cell membrane separates the interior of the cell from the extracellular liquid and in this way, acts as a *capacitor*. If an input current - which can account as a sensory stimulus - I_{stim} is injected, it may add a certain amount of charge on the capacitor or either leak through the channels in the cell membrane. Each channel is represented as a *resistor*, but usually, instead of talking about resistances, the neuroscience community considers *conductances*. Each of the three considered channels has its own conductance, g_{Na}, g_K, g_L. In the original model, g_L is constant, while g_{Na} and g_K are not fixed and depend on whether the ion channel is open or closed. Because of this ion transport through the cell membrane, different ion concentrations between the inside and the outside arise, this generates

a potential, i.e. the *Nernst potential*, which is represented by a battery in Figure 4.1. Since the Nernst potential is different for each ion type, we define separate batteries for sodium, potassium and leak, with voltages E_{Na}, E_K and E_L respectively.

We can now translate this electrical circuit into mathematical equations. The conservation of electric charge implies that the applied current I_{stim} can be split in two pieces: a capacitive current I_C, which charges the capacitor C, and other components I_m which pass through the ion channels. This leads to:

$$I_{stim}(t) = I_C(t) + \sum_m I_m(t)$$

where the sum is over all the ion channels. From the definition of capacity we can rewrite the charging current as $I_C = C \cdot dV/dt$. Hence:

$$C\frac{dV}{dt} = -\sum_m I_m(t) + I_{stim}(t) \tag{4.1}$$

where V in biological terms represents the voltage across the membrane. By employing *Ohm's law* we can explicit the leak current as $I_L = g_L(V - E_L)$, where (V_{EL}) is the voltage at the leak resistor. As a physicist you would expect to replicate this procedure for the sodium as well as for the potassium channel. In fact the mathematics are analogous but the exact Ohm's law would not fit the experimental data of the giant squid axon: the peculiarity of Hodgkin and Huxley's work has been to introduce additional gating variables m, n and h to model the probability that a channel is open at a given moment in time. Variables m and h, combined together, control sodium channels while n controls potassium channels. In this way the sodium current would be $I_{Na} = g_{Na}m^3h(V - E_{Na})$ while the potassium current $I_K = g_K n^4(V - E_K)$. The sum of currents becomes:

$$\sum_m I_m(t) = g_{Na}m^3h(V - E_{Na}) + g_K n^4(V - E_K) + g_L(V - E_L) \tag{4.2}$$

On the other side each of the three gating variables $y(t) = \{n(t), m(t), h(t)\}$ satisfies first-order kinetics:

$$\frac{dy}{dt} = \alpha_y(V(t))\big[1 - y(t)\big] - \beta_y(V(t))y(t) \tag{4.3}$$

where $\alpha_y(V)$ and $\beta_y(V)$ are nonlinear functions. For example, for n in our simulation which results in Figure 4.2 we have:

$$\alpha_n(V) = \frac{0.1 - 0.01V}{e^{1-0.1V} - 1} \qquad \beta_n(V) = \frac{0.125}{e^{0.125V}} \tag{4.4}$$

These formulae are analogous for the other two gating variables.

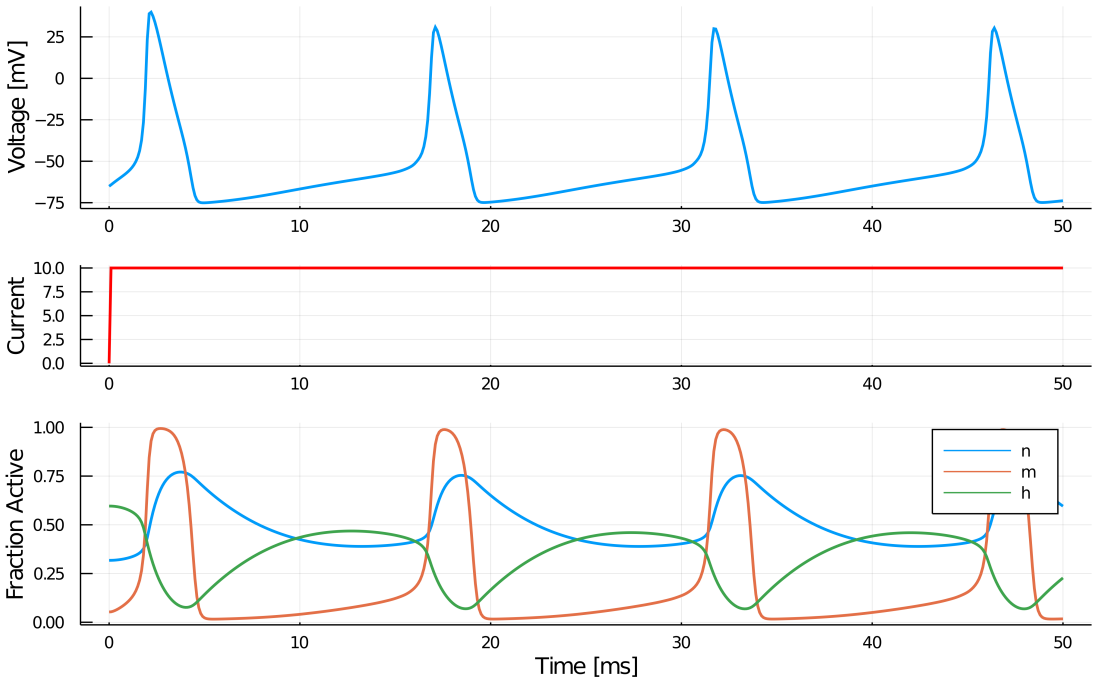

Figure 4.2: *top* membrane potential V of a Hodgkin-Huxley neuron; *middle* input current I_{stim}, in this case it is constant; *bottom* gating variables dynamics.

In the end the Hodgkin-Huxley model is one of the most biologically plausible neuron models, even though some caution is needed when trying to simulate a large number of HH neurons on a computer, see 4.3 for a comparison with other models. In the next section, we will show how, for our needs, it is possible to reduce the HH model in a similar fashion to what Fukai & Tanaka achieved in their paper [14] by keeping, at the same time, all the dynamical properties, e.g. bifurcations, in the phase space. This then provides a stronger biophysical basis for the neuron models used in our WLC analysis and its application to exploration in animals.

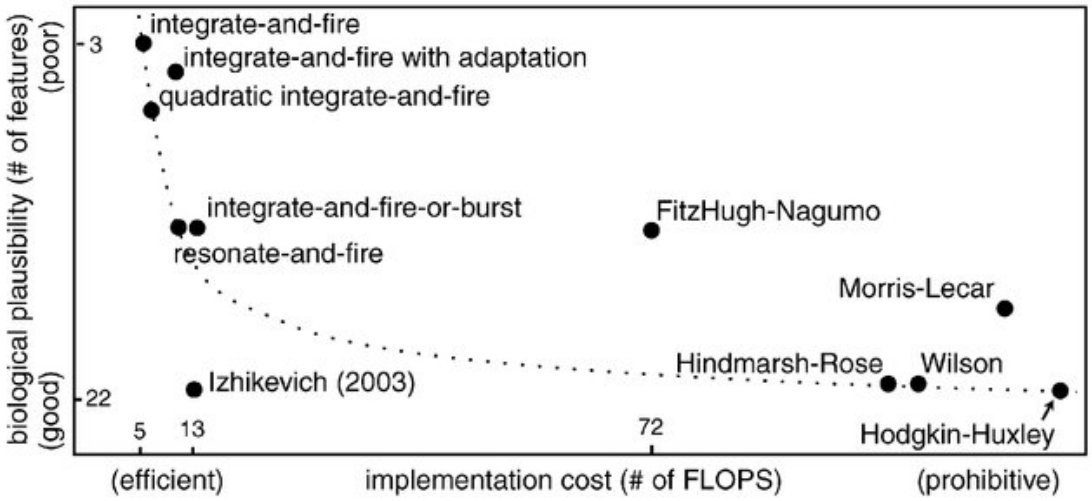

Figure 4.3: Biological plausibility vs computational efficiency of different neuron models taken from [32]

4.2 Hodgkin-Huxley Revisited

We would like to consider a minimal network which embodies all the necessary requirements to show a WLC behavior, and on the other side, we are particularly interested in the class of dynamical systems that describe typical motifs (building blocks) of complex neural circuits: in order to satisfy these requirements we decided to consider the most common neuronal circuit [33], made up by three coupled inhibitory HH neurons.

For the first time in [34], a sequence of bifurcations that leads to the appearance of an heteroclinic cycle has been observed in the high dimensional phase space of a system of HH-neurons. In particular, the most impressive result, which we replicate here, is the comparison between the bifurcation sequence from tonic activity to burst generation in a network of three HH neurons and the sequence of bifurcations of a time averaged rate model of the same network - i.e. Lotka-Volterra model, which showed that these sequences are the same.

The network consists of three HH neurons (as in Figure 4.4) which are connected by inhibitory synapses - i.e. neurons are nodes, synapses are links in our network. For each individual neuron (4.1) holds but we introduce another term, a synaptic

current I_{syn} so that we get:

$$C\frac{dV_i}{dt} = +I_{stim}(t) - I_{Na}(t) - I_K(t) - I_L(t) - I_{syn}(t) \tag{4.5}$$

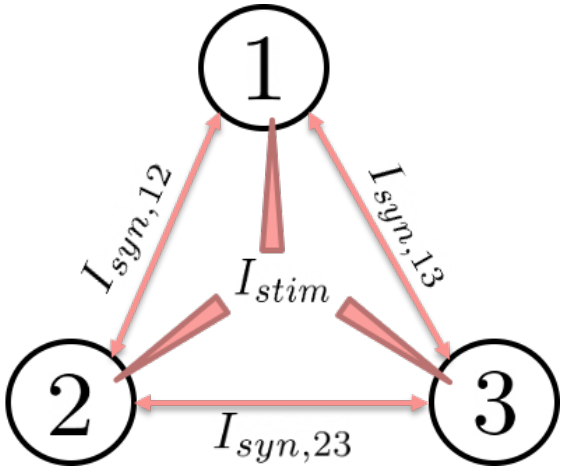

Figure 4.4: Three Hodgkin Huxley neurons, connected by inhibitory synapses which constitute our motif of choice. Synapses strength are symmetric, e.g. $(I_{syn,12} \equiv I_{syn,21})$

The synaptic current onto neuron j is the linear sum of all incoming synapses, $I_{syn,j} = \sum_i I_{syn,ji}$ where individual currents are modelled as in [35], [36]:

$$\begin{cases} I_{syn,ji} = g_{ji} S_i (V_j - V_{rev}) \\ \tau \frac{dS_i}{dt} = (R_i - \kappa S_i) \frac{S_{max} - S_i}{S_{max}} \\ \tau \frac{dR_i}{dt} = \Theta(V_i - V_{th}) - R_i \end{cases} \tag{4.6}$$

where R_i is a measure of the amount of neurotransmitter released presynaptically, S_i is the fraction of postsynaptically bound neurotransmitter, V_{th} is the threshold potential for neurotransmitter release, τ is the synaptic time scale, S_{max} is the maximal fraction of postsynaptically bound transmitter, κ is the relative rate of transmitter binding and unbinding and Θ is the Heaviside function.

We will now reduce this model to a rate model, which is indeed very similar to the Fukai & Tanaka model. The presynaptic release of neurotransmitter, R_i is driven by spikes. In particular, we will focus on x_i, the spiking rate of neuron i. We can calculate the average release r_i of the presynaptic spike train by a rate equation, which takes the form:

$$\tau \frac{dr_i}{dt} = f(x_i) - r_i \tag{4.7}$$

where f is a function of the firing rate of neuron i. It is possible to determine f by requiring that $r_i = R_i$ [34] for a tonic presynaptic train:

$$\tau \frac{dr_i}{dt} = \frac{1 - e^{(-\tau_{spike}/\tau)}}{1 - e^{-1/(x_i\tau)}} - r_i \tag{4.8}$$

where τ_{spike} is the spike width measured at $V_i = 0$ mV. The HH neuron model has a clear relation between spike rate and input current - f-I curve - , which can be approximated (see Figure 4.5) by:

$$x_i \simeq x_0 \Big[max\{(I_{syn,i} + I_{stim} - I_0)/nA, 0\} \Big]^{\alpha} \tag{4.9}$$

where I_0, α and x_0 come out from a least squares fit. In this case we can see how such a model is more effective than linear f-I curves. Moreover, V_i is approximately constant, such that we can substitute V_{rest} for it, and the synaptic current becomes:

$$I_{syn,j} = -\sum_i g_{ji} s_i (V_{rest} - V_{rev}) = -\sum_i \hat{g}_{ji} s_i \tag{4.10}$$

where s_i is the averaged version of S_i, and $\hat{g}_{ji}$ is a constant. By denoting $\tilde{g}_{ij} = \hat{g}_{ij}/\mu A$, $\tilde{I} = (I_{stim} - I_0)/\mu A$, we get:

$$x_i = x_0 \left[\tilde{I} - \sum_j \tilde{g}_{ij} s_j \right]_+^{\alpha} \tag{4.11}$$

where $[...]_+^{\alpha} \equiv (max\{...,0\})^{\alpha}$. By inserting (4.11) in (4.8):

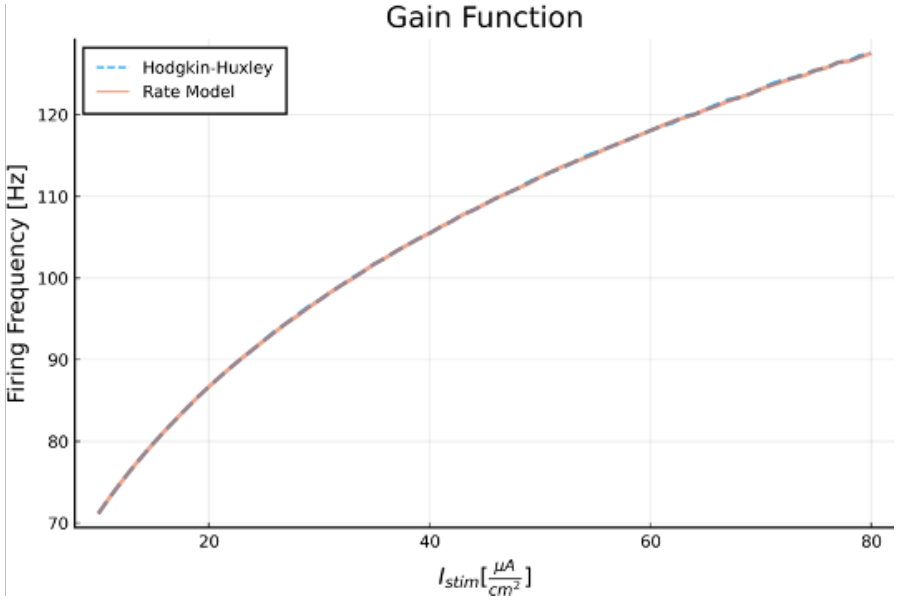

Figure 4.5: f-I curve - i.e. gain function - x of the HH neuron, which is fitted almost perfectly by (4.9)

$$\tau \frac{dr_i}{dt} = \frac{1 - e^{-\tau_{spike}/\tau}}{1 - e^{-(x_0[\tilde{I} - \sum_j \tilde{g}_{ij} s_j]_+^\alpha \tau)^{-1}}} - r_i$$

$$\simeq \tilde{x}_0 \left[\tilde{I} - \sum_j \tilde{g}_{ij} s_j \right]_+^\alpha \tau - r_i$$

where we have employed the truncated Taylor expansion for $e^x \simeq 1 + x$ for small values of x, and $\tilde{x}_0 = [1 - e^{-\tau_{spike}/\tau}] x_0$. In the end we get an approximated model of the form:

$$\begin{cases} \tau \frac{ds_i}{dt} = (r_i - \kappa s_i) \frac{S_{max} - s_i}{S_{max}} \\ \\ \tau \frac{dr_i}{dt} = \tilde{x}_0 \left[\tilde{I} - \sum_j \tilde{g}_{ij} s_j \right]_+^\alpha \tau - r_i \end{cases} \tag{4.12}$$

The effectiveness of this approximated model can be seen in Figure 4.6, where,

for non-symmetric g_{ij}, after a short transient the three HH neurons (*left*) fire sequentially with a fixed peak-to-peak temporal spacing. On the other side, the three coupled rate neurons (*right*) fire sequentially with the same peak-to-peak temporal spacing. From the point of view of rate coding, where the information content is brought by the frequency of spikes, these two systems are completely equivalent.

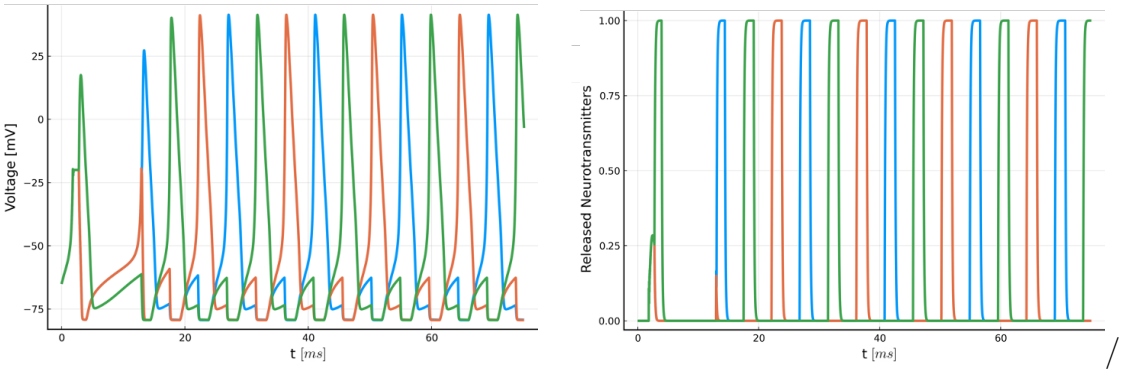

Figure 4.6: *Left:* Aggregated plot for the HH spiking neuronal motif, each color represent a specific neuron. As you can see, there is a precise sequential switching which is the effect of the heteroclinic loop; *right:* Aggregated plot for the rate model motif, again each color represent a specific neuron. In this case we still have a sequential switching and, more importantly, we can see that the spike trains are the same in terms of timing.

A more powerful demonstration of equivalence between the two systems has been carried out in [34], where they start by considering couplings with an equal strength $g_{ij} = g_{ji} = g$. In this view, g acts as a control parameter for our dynamical system, in particular for strong competition ($g > 30nS$), the system shows multistability. In the phase space, three fixed points - corresponding to a WTA behavior - arise and the boundaries of the basins of attraction of these attractors are the separatrices of the saddles. The observed phenomena in the three HH neurons motif are identical to the ones in the three rate neurons, see Figure 4.7.

As we have previously stated, having symmetric interactions - i.e. $g_{ij} = g_{ji}$ - between neurons cannot lead to WLC behavior, and thus we cannot observe an heteroclinic structure in the phase space. We can introduce asymmetric connections by specifying two different values for g, for each direction of the synapses - we are basically considering a directed network now -, g_1 and g_2. For increasing asymmetry, at a critical value of the ratio g_1/g_2 saddles and fixed points merge together, leading to the appearence of a heteroclinic cycle which presents a characteristic sequential

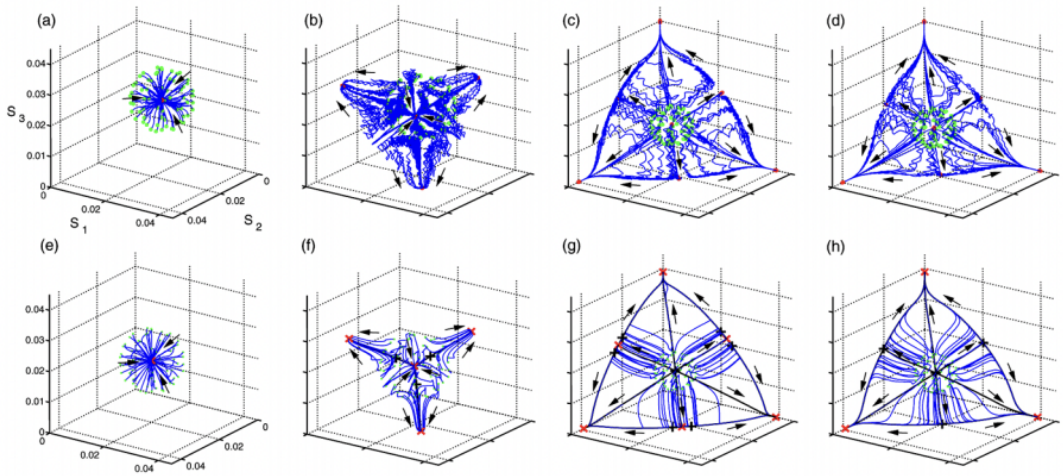

Figure 4.7: *Top*: Bifurcations of the three HH neurons motif for symmetric reciprocal interaction of increasing strength. Axes correspond to the three synaptic activation variables S_1, S_2, S_3. *Bottom*: Bifurcations of the three rate neurons motif for symmetric reciprocal interaction of increasing strength. Axes correspond to the three synaptic activation variables s_1, s_2, s_3. Synaptic conductances, as in [34], , (a) $g = 10nS$, (b) $g = 30nS$, (c) $g = 50nS$, (d) $g = 60nS$, (e) $g = 30nS$, (f) $g = 40nS$, (g) $g = 51.4nS$, (h) $g = 60nS$

switiching activity, as in Figure 4.6.

Chapter 5

Sequential Spatial Memory

Even though sequential learning and memory have been studied for a long time, little is known about dynamical principles of learning and memorizing multiple events with some specific temporal order in neural systems. The Winnerless Competition principle can be framed as a mechanism for explaining sequential memory by chaining a series of events. In [37] a two-layer neuronal network, which works under the guidance of a WLC dynamics, has been proposed for this task. This specific model, after a learning phase, is able to retrieve a prerecorded sequence of patterns. The essence of the idea behind this work is that the sequential memory is encoded in a multidimensional dynamical system with a heteroclinic trajectory connecting a sequence of saddle points which individually represent a memory - i.e. a pattern - to be stored. In spatial navigation, each saddle point in the phase space could correspond to a specific pattern - i.e. a landmark or a target - in the physical space. All saddle points are connected by a one-dimensional stable heteroclinic orbit, which guarantees the global stability of this structure.

From a biological perspective, it is well established that the hippocampus plays a key role in processing the information related to the representation of space. One of the most spectacular results of this role are the so-called *place cells*, which fire whenever an animal is in a certain spatial location. The discovery of place cells lead to a Nobel prize, in [38] more details on this finding are available. This work led to a paradigm for spatial memory, named the *cognitive map* [39], which concentrated and conditioned several years of experimental research.

Even though this result is definitely well-grounded, our brain might employ other strategies for spatial navigation at the same time. One way could be the alternative concept of thinking about a trajectory as a linked collection of stored episodes, where each episode is made up by a sequence of events which may include different features of the environment. In this view, each event is represented by the

activity of a specific hippocampal cell. In this viewpoint we are going to talk about *episodic memory*, a framework which is favored by different neurophysiological findings [40], [41].

5.1 A WLC-Based Model

A dynamical model of sequential spatial memory should be built on the following facts:

1. There should be a neat separation between neurons that respond to specific stimuli, i.e. *sensory neurons* (SNs) and hippocampal cells - biologically they would correspond to CA1 and CA3 regions -, i.e. *principal neurons* (PNs).

2. SNs are not connected to each other while PNs are coupled by inhibitory synapses

3. Synapses between PNs and between SNs and PNs show a reinforcement learning mechanism named *Hebbian long-term potentiation* (LTP) [42]

By following these three features here we propose, along [37], a two-layer dynamical model of sequential spatial memory (SSM) as in Figure 5.1.

Based on this network, we will try to answer the following questions:

- How is a certain event recorded in the structure of such a network?

- What kind of competitive dynamics forces individual Principal Neurons to fire sequentially?

The first goal is to learn a projection map, the transformation which links the heightened activity of SNs to the activity of one PN. The second goal is to learn the temporal sequence of events, which can be done thanks to Hebbian LTP. The phase space of such a system shows WLC behavior, which guarantees the stability of learning.

In order to satisfy the first objective, we employ a similar structure to the one of the *normal form projection algorithm* (NFPA) [43]. In this model, the dynamics of the network is framed in terms of the normal form equations which corresponds to different patterns stored in the system. In [43], Lotka-Volterra equations for example can be considered as a special set of normal form equations, which are finally connected to the Fukai & Tanaka model and to the viewpoint of neurons as competitive systems.

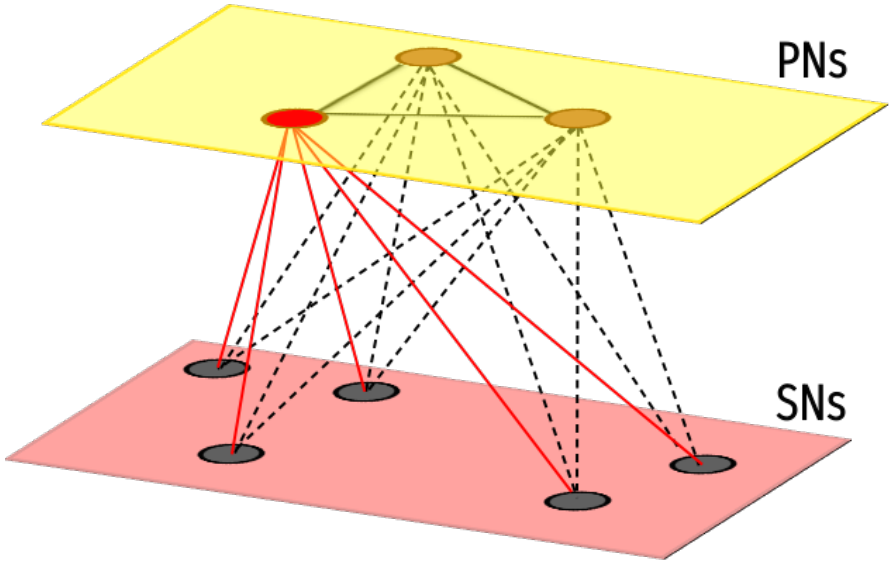

Figure 5.1: A two-layer network, the top layer is made of Principal Neurons (PNs), which are connected between each other by inhibitory synapses and projects their activity into the bottom layer, made of Sensory Neurons (SNs). SNs are not connected between each other but they only "sense" the environment.

Let us consider a two-layer network of N_s sensory neurons x_i and N_p principal neurons a_i. We assume that SNs do not have their own dynamics and are slaved to external stimuli in the *learning regime* or to PNs in the *retrieval regime*. In the learning regime, sensory neurons perceive a set of binary - consisting of 0s and 1s - stimuli, $x_i = I_i$. Indeed, during the retrieval phase, $x_i = \sum_{j=1}^{N_p} P_{ij} a_j$ with P being the $N_s \times N_p$ projection matrix of connections between SNs and PNs. On the other side PNs are driven by SNs in the learning phase but they also have their own dynamics due to inhibitory connections. We can write down the equations for the amplitudes of PNs:

$$\dot{a}_i = a_i - a_i \sum_{j=1}^{N_p} V_{ij} a_j + \alpha a_i \sum_{j=1}^{N_s} P_{ij}^T x_j + \xi(t) \tag{5.1}$$

where the parameter α controls the learning ($\alpha = 1$) and retrieval ($\alpha = 0$) regimes and $\xi(t)$ represents an external perturbation which is modelled as white noise extracted from a uniform distribution between 0 and $\sigma = 10^{-4}$.

There are two other learning processes which are essential for our model: learning

the projection matrix P which connects a group of sensory neurons to a single principal neuron. These sensory neurons represent the pattern we would like to store on a higher level; learning the *competition matrix* V which controls the temporal ordering of the stored events lets the sequential memory work.

The dynamics of the projection matrix is on a slower timescale with respect to (5.1):

$$\dot{P}_{ij} = \epsilon a_i(\beta x_i - P_{ij}) \tag{5.2}$$

where $\epsilon = 0.01 \ll 1$. For the initialization of P, we assume that all the entries are nearly identical, $P_{ij} = 1 + \eta_{ij}$, where η_{ij} are small perturbations such that $\sum_j \eta_{ij} = 0$ and $< \eta_{ij}^2 >= \eta_0^2 \ll 1$. For V we assume an initial WTA behavior, which basically means that $V_{ii} = 1$ and $V_{ij} = V_0 < 1$ for $i \neq j$.

Let us say that we want to memorize a specific pattern **A**. The sensory neurons perceive a set of input A_i corresponding to pattern **A**. Such stimuli make each of the SNs in one of the following states: excited - $A_i = 1$ - or inactive - $A_i = 0$. PNs are initialized in a fully excited state - $a_i(0) = \sum_j P_{ij} A_j$. At the end of the learning phase, only one of the PNs, which corresponds to the maximum $a_i(0)$, will be active. Since P is initialized randomly, the maximum $a_i(0)$ is in turn random. In (5.2) we can see how P_{ij}'s corresponding to quiescent a_i's do not change. The result of this procedure is such that the pattern will be recorded in one of the rows of P, while other rows will not change.

In case we want to store a second pattern **B**, which is different from **A**, we can repeat the same procedure as before. Firstly, we initialize the PNs as $a_i(0) = \sum_j P_{ij} B_j$. Since pattern **A** is already stored, pattern **B** will excite the neuron responsible for **A** in a weaker manner. Competition will lead to another different neuron for storing **B**. This basically means that we can store as many patterns as PNs.

The competition matrix determines the logical order of patterns. The goal is to record in V the transition between pattern **A** and pattern **B** by modifying the element V_{BA}. The dynamics of the elements of the competition matrix are controlled by the following delay differential equation:

$$\dot{V}_{ij} = \epsilon a_i(t) a_j(t - \tau)(V_1 - V_{ij}) \tag{5.3}$$

where $V_1 < 1$ is an asymptotic value. Only the matrix elements corresponding to $a_i(t) \neq 0$ and $a_j(t - \tau) \neq 0$ will change, and, given the fact that only one PN at a time is active, only one of the V_{ij} is changing. The result is that an arbitrary sequence of patterns can be stored and retrieved.

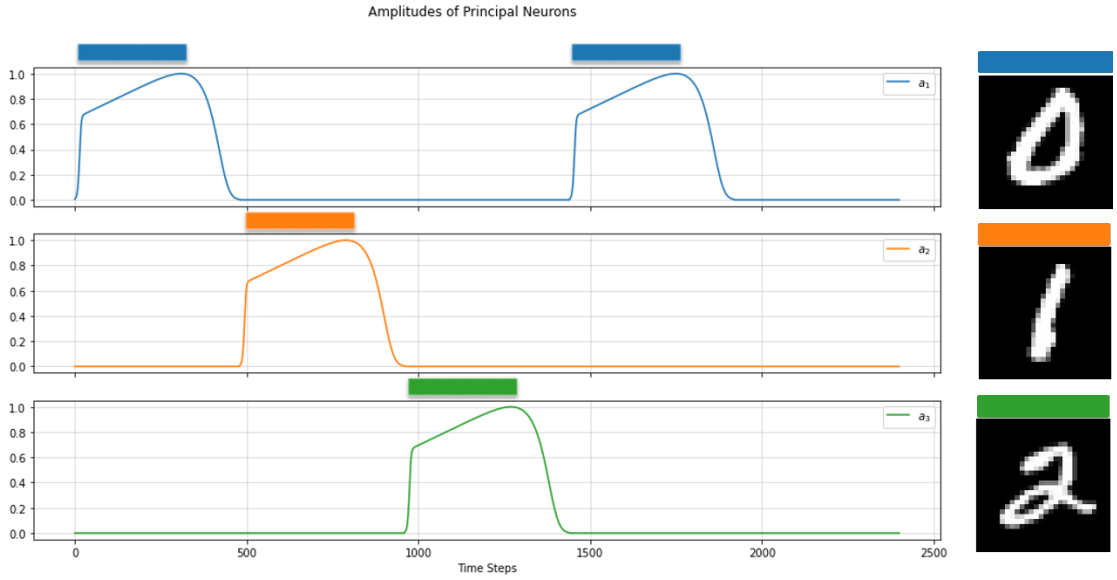

Figure 5.2: PNs amplitudes in the learning phase: patterns - i.e. MNIST handwritten digits - are shown as sensory stimuli for a fixed amount of time steps - i.e. 350 timesteps in our case - followed by a null stimulus, i.e. a zero-vector. Each of the PNs is associated with a specific input. We ensure the birth of a stable heteroclinic contour by closing the loop with the presentation of the last input being the same as the first one. In the retrieval phase the plot would be the same, but with the only difference that by presenting to SNs only the first input, the system will retrieve the entire sequence.

Chapter 6

Conclusions

Up to here we have covered all the possible facets of spatial navigation: from real world data, to descriptive modeling of animal foraging, up until a possible phenomenological model which is based on neuronal circuits dynamics: the WLC principle. It is time to close the circle and understand whether there is a relation between WLC and Levy exploration strategies.

In [44] a concrete effort is made in trying to link WLC and Levy strategies. In particular, in this work, WLC is proposed as the neuronal codification mechanism that allows Levy-like searching strategies due to the fact that it is possible to show multifractality properties in residence times, when the system crosses each saddle in the phase space. They propose two different ways in order to extract the hidden multifractality from a rate model system as well as from experimental neuronal recording data: de facto confirming the validity of the WLC principle in real-world scenarios. In the end, the Winnerless Competition principle, not only induces the existence of globally stable dynamical structures, i.e. stable heteroclinic sequences, but eventually shows multifractality properties, which are relevant to guarantee the existence of multi-scale phenomena.

6.1 Final Remarks

In this thesis we have presented an itinerary which aims at connecting apparently distant topics in order to propose a framework for spatial sequential memory. We have showed how everything relates back to inhibitory synapses and competition among neurons and we have directly mapped Fukai & Tanaka's work into the Winnerless Competition principle by means of reduced neuron model.

From another perspective, what we have done still presents some limitations. For example, the system we have considered admits a fully connected principal neurons layer and it is not yet clear how to deal with multiple populations of principal neurons, even though some results in this direction are encouraging [45]. Another consideration worth to mention is the fact that the Spatial Sequential Memory model in chapter 5 works with two separate phases: *learning* and *retrieval*. Such a separation in learning and retrieving memories is not biologically plausible and it is something that we are going to tackle in the near future.

Appendix A

Linear Stability (of Nonlinear Dynamical Systems)

Let's consider the dynamics of a system of nonlinear differential equations:

$$\dot{\vec{x}} = \vec{F}(\vec{x}) \qquad \vec{x} \in \mathbb{R}^N \tag{A.1}$$

A fixed point $\vec{x}_0 \in \mathbb{R}^N$ is a point such that $\vec{F}(\vec{x}_0) = 0$. Let's understand what happens around a fixed point for infinitesimal perturbations:

$$\vec{x} = \vec{x}_0 + \epsilon\vec{z} \tag{A.2}$$

By definition we get:

$$\dot{\vec{x}}_0 + \epsilon\dot{\vec{z}} = \vec{F}(\vec{x}_0 + \epsilon\vec{z}) \tag{A.3}$$

which eventually leads, by considering each vector elements and the fact that $\dot{\vec{x}}_0 = 0$, to:

$$\epsilon\dot{z}_i = F_i(\vec{x}_0) + \epsilon\left.\frac{\partial F_i}{\partial x_j}\right|_{\vec{x}_0} z_j + o(\epsilon^2) \tag{A.4}$$

Since $F_i(\vec{x}_0) = 0$ we get (first order in ϵ):

$$\dot{z}_i = \left.\frac{\partial F_i}{\partial x_j}\right|_{\vec{x}_0} z_j = A_{ij} z_j \tag{A.5}$$

where the matrix made up of A_{ij} elements, i.e. $\mathbf{A}$, is nothing but the *Jacobian* matrix.

The linear stability test depends on the real part of **A**'s eigenvalues λ_i - i.e. $Re(\lambda_i)$. In fact, we have:

- $\vec{x_0}$ is linearly stable if and only if $Re(\lambda_i) \leq 0$
- $\vec{x_0}$ is unstable if and only if $Re(\lambda_i) > 0$

Appendix B

Why May-Leonard? Carrying Simplex Existence (Smale's Construction)

Let's consider a general model of **total competition** (more general than the specific May-Leonard system):

$$\dot{x}_i = x_i M_i(x) = F_i(x) \tag{B.1}$$

where M_i is smooth. We pose two hypotheses:

- **H1** For all pairs i, j we have $\frac{\partial M_i}{\partial x_j} < 0$ when $x_i > 0$ (total competition);
- **H2** There is a constant K such that for each $i, M_i(x) < 0$ if $|x| > K$

H1 basically means that, for all i, j if $x_i > 0$:

$$\frac{\partial \dot{x}_i}{\partial x_j} = x_i \frac{\partial M_i(x)}{\partial x_j} < 0 \tag{B.2}$$

i.e. competition for resources. While **H2** means that there are finite resources and thus, there's an upper bound on population growth.

Smale has been able to show [46] that if our system satisfies (10) and both **H1** and **H2**, its long term dynamics lies on a simplex and obeys $\dot{x} = H(x)$ on that simplex, where H is any smooth vector field of our choice.

Here we follow [46] [47] and we show a quick demonstration. Let $\Delta_1 = \{x \in \mathbb{R}^n_{\geq 0} : ||x||_1 = 1\}$ be the standard probability simplex with tangent space $\Delta_0 =$

$\{x \in \mathbb{R}^n : \sum_{i=1}^n x_i = 0\}$. Let $H_0 : \Delta_1 \to \Delta_0$ be a smooth vector field on Δ_1 whose components can be written as $H_{0i}(x) = x_i g_i(x)$ and $H : \mathbb{R}^n_{\geq 0} \to \Delta_0$ any smooth map which agrees with H_0 on Δ_1.

Now, let $\eta(s) : \mathbb{R} \to \mathbb{R}$ be any smooth function which is 1 in a neighborhood of 1 and 0 if $s \leq \frac{1}{2}$ or $s \geq \frac{3}{2}$.

For any $\epsilon > 0$ we define M_i on $\mathbb{R}^n_{\geq 0}$ by:

$$M_i(x) = 1 - ||x||_1 + \epsilon\eta(||x||_1)g_i(x) \tag{B.3}$$

We can check that for each i, j:

$$\frac{\partial M_i}{\partial x_j} = -1 + \epsilon\eta'(||x||_1)g_i + \epsilon\eta(||x||_1)\frac{\partial g_i}{\partial x_j} < 0 \tag{B.4}$$

for small enough ϵ. Now we have $\frac{d||x||_1}{dt} = \sum_{i=1}^n \dot{x}_i = ||x||_1(1 - ||x||_1)$, which is the logistic equation.

Thus Δ_1 is forward invariant and any point in $\mathbb{R}^n_{\geq 0} \setminus \{0\}$ is attracted to Δ_1. On Δ_1 we have:

$$M_i(x) = 1 - ||x||_1 + \epsilon\eta(||x||_1)g_i(x) = \epsilon g_i(x) \tag{B.5}$$

so that the dynamics on the attractor is $\dot{x}_i = x_i \epsilon g_i(x) = \epsilon h_i(x)$ □

A (bounded) totally competitive system with unstable origin has a unique invariant manifold that attracts the dynamics [48] (i.e. first orthant minus the origin). In the May-Leonard system, the invariant manifold can be explicitly found, and all orbits except the origin are attracted to it. Exceptionally, the dynamics on the simplex, in that case, is canonically Hamiltonian and all orbits are periodic.

Here we consider the same total competition model, but we enforce the hypothesis set by adding:

- **H3** $M_i(0) > 0$

This last condition makes the origin 0 a repelling steady state. Orbits are bounded, which implies that the basin of repulsion of 0 in $\mathbb{R}^n_{\geq 0}$ is bounded too. The boundary of the basin of repulsion is called the **Carrying Simplex** and is denoted by Σ. From Hirsch [49] we have the following theorem:

Theorem 1 (The Carrying Simplex). Given (10) every trajectory in $\mathbb{R}^n_{\geq 0} \setminus \{0\}$ is asymptotic to one in Σ is a Lipschitz submanifold, everywhere transverse to all strictly positive directions, and homeomorphic to the probability simplex.

Given this theorem, totally competitive n-dimensional Lotka-Volterra systems eventually evolve like $n-1$ dimensional systems.

By going back to the *May-Leonard system* we can understand how *Smale's Construction* turns out to be useful.

B.0.1 Hamiltonian Dynamics ($\alpha + \beta = 2$)

Here we show that for this very special case, where $\alpha + \beta = 2$, it is possible to rephrase the May-Leonard system as a canonical Hamiltonian system.

Let's start by defining a biologically motivated *Lyapunov function*:

$$V(x, y, z) = xyz \tag{B.6}$$

Then

$$\begin{aligned}
\frac{dV}{dt} &= xyz\left(\frac{\dot{x}}{x} + \frac{\dot{y}}{y} + \frac{\dot{z}}{z}\right) \\
&= V((1 - x - \alpha y - \beta z) + (1 - \beta x - y - \alpha z) + (1 - \alpha x \beta y - z)) \\
&= V(3 - (x + y + z) - (\alpha + \beta)(x + y + z)) \\
&= 3V\left(1 - \frac{(1 + \alpha + \beta)}{3}(x + y + z)\right) \\
&\doteq 3V(1 - (x + y + z))
\end{aligned}$$

Moreover

$$\begin{aligned}
\frac{d(x + y + z)}{dt} &= x + y + z - x^2 - y^2 - z^2 - (\alpha + \beta)(xy + xz + yz) \\
&= (x + y + z)(1 - (x + y + z)) - (\alpha + \beta - 2)(xy + xz + yz)) \\
&\doteq (x + y + z)(1 - (x + y + z))
\end{aligned}$$

Thus if $(x_0, y_0, z_0) \in \mathbb{R}^3 \setminus (0,0,0)$ we have that: for $t \to \infty$, $x(t) + y(t) + z(t) \to 1$.

Note that WLC behaviour is guaranteed up until we have $\alpha > 1$ and $\beta < 1$, see [23].

All orbits end up on the simplex Δ_1. On Δ_1 we have:

$$\frac{dV}{dt} = 3V(1-(x+y+z)) = 0$$

On Δ_1 we might eliminate z since here $z = 1-x-y$:

$$\dot{x} = x(1-x-\alpha y-\beta(1-x-y)) = \frac{(\alpha-\beta)}{2}(1-x-2y)x$$
$$\dot{y} = y(1-\beta x-y-\alpha(1-x-y)) = -\frac{(\alpha-\beta)}{2}(1-2x-y)y$$

Moreover:

$$\begin{aligned} div(\dot{x},\dot{y}) &= \frac{(\alpha-\beta)}{2}\Big((1-x-2y)-x\Big) - \frac{(\alpha-\beta)}{2}\Big((1-2x-y)-y\Big) \\ &= \frac{(\alpha-\beta)}{2}(1-2x-2y-1+2x+2y) \\ &= 0 \end{aligned}$$

Thus, we have a canonical Hamiltonian system with the following Hamiltonian function:

$$H(x,y) = \frac{(\alpha-\beta)}{2}(1-x-y)xy \tag{B.7}$$

B.0.2 Hamiltonian Dynamics ($\alpha+\beta>2$)

In the general case, $\alpha+\beta>2$. Let's declare a new parameter: $\gamma = \alpha+\beta-2$. So that now we have:

$$\frac{d(x+y+z)}{dt} = (x+y+z)(1-(x+y+z)) + \gamma(xy+xz+yz))$$

And, by recovering (22) we have:

$$\frac{dV}{dt} = V((3+\gamma)(1-x+y+z)-\gamma)$$

Now we can assume that the products of terms of order xy, yz, xz make a negligible contribution asymptotically, for large t [24]. In this case, the asymptotic solution is:

$$ln\left(\frac{V(t)}{V(t_0)}\right) \to -\gamma(t - t_0)$$

$$V(t) \to ke^{-\gamma(t)} \tag{B.8}$$

where k is a constant. Note that (24) lies on the plane $x + y + z = 1$, but the product of the 3 populations becomes exponentially small as time goes on. The system comes ever closer to the lines $x + y = 1$, $y + z = 1$, $x + z = 1$, but it never converges on any single point, because there are no asymptotically stable points for α, β values in this domain. This means that from an Hamiltonian perspective we are back in the previous case.

Bibliography

[1] James J Jun, André Longtin, and Leonard Maler. «Long-term Behavioral Tracking of Freely Swimming Weakly Electric Fish». eng. In: *Journal of Visualized Experiments* 85 (2014). ISSN: 1940-087X (cit. on pp. 2, 4).

[2] James J. Jun, André Longtin, and Leonard Maler. «Active sensing associated with spatial learning reveals memory-based attention in an electric fish». In: *Journal of Neurophysiology* 115.5 (2016). PMID: 26961107, pp. 2577–2592. DOI: 10.1152/jn.00979.2015. eprint: https://doi.org/10.1152/jn.00979.2015. URL: https://doi.org/10.1152/jn.00979.2015 (cit. on p. 3).

[3] Jia Deng, Wei Dong, Richard Socher, Li-Jia Li, Kai Li, and Fei-Fei Li. «ImageNet: A large-scale hierarchical image database.» In: *CVPR*. IEEE Computer Society, 2009, pp. 248–255. ISBN: 978-1-4244-3992-8. URL: http://dblp.uni-trier.de/db/conf/cvpr/cvpr2009.html#DengDSLL009 (cit. on p. 5).

[4] Alexander Mathis, Pranav Mamidanna, Kevin M Cury, Taiga Abe, Venkatesh N Murthy, Mackenzie Weygandt Mathis, and Matthias Bethge. «DeepLabCut: markerless pose estimation of user-defined body parts with deep learning». eng. In: *Nature neuroscience* 21.9 (2018), pp. 1281–1289. ISSN: 1097-6256 (cit. on pp. 5, 6).

[5] K. He, X. Zhang, S. Ren, and J. Sun. «Deep Residual Learning for Image Recognition». In: *2016 IEEE Conference on Computer Vision and Pattern Recognition (CVPR)*. 2016, pp. 770–778. DOI: 10.1109/CVPR.2016.90 (cit. on p. 5).

[6] Eldar Insafutdinov, Leonid Pishchulin, Bjoern Andres, Mykhaylo Andriluka, and Bernt Schiele. «DeeperCut: A Deeper, Stronger, and Faster Multi-person Pose Estimation Model». In: *Computer Vision – ECCV 2016*. Ed. by Bastian Leibe, Jiri Matas, Nicu Sebe, and Max Welling. Cham: Springer International Publishing, 2016, pp. 34–50. ISBN: 978-3-319-46466-4 (cit. on p. 5).

[7] E. P Raposo, H. Eugene Stanley, M. G. E da Luz, G. M Viswanathan, Shlomo Havlin, and Sergey V Buldyrev. «Optimizing the success of random searches». eng. In: *Nature (London)* 401.6756 (1999), pp. 911–914. ISSN: 0028-0836 (cit. on pp. 7, 9, 10).

[8] S. V Buldyrev, E. J Murphy, V Afanasyev, P. A Prince, H. E Stanley, and G. M Viswanathan. «Lévy flight search patterns of wandering albatrosses». eng. In: *Nature (London)* 381.6581 (1996), pp. 413–415. ISSN: 0028-0836 (cit. on p. 7).

[9] Micheal F Shlesinger, George M Zaslavsky, and Uriel Frisch. *Lévy Flights and Related Topics in Physics: Proceedings of the International Workshop Held at Nice, France, 27–30 June 1994*. eng. Vol. 450. Lecture Notes in Physics. Berlin, Heidelberg: Springer Berlin Heidelberg, 1995. ISBN: 9783662140475 (cit. on p. 8).

[10] Stephen Grossberg. «Contour Enhancement, Short Term Memory, and Constancies in Reverberating Neural Networks». eng. In: *Studies in applied mathematics (Cambridge)* 52.3 (1973), pp. 213–257. ISSN: 0022-2526 (cit. on p. 12).

[11] M. A Cohen and S Grossberg. «Absolute stability of global pattern formation and parallel memory storage by competitive neural networks». eng. In: *IEEE transactions on systems, man, and cybernetics* SMC-13.5 (1983), pp. 815–826. ISSN: 0018-9472 (cit. on p. 12).

[12] E. D Adrian and Yngve Zotterman. «The impulses produced by sensory nerve-endings: Part II. The response of a Single End-Organ». eng. In: *The Journal of physiology* 61.2 (1926), pp. 151–171. ISSN: 0022-3751 (cit. on p. 13).

[13] K. I. Naka and W. A. H. Rushton. «S-potentials from luminosity units in the retina of fish (Cyprinidae)». eng. In: *The Journal of physiology* 185.3 (1966), pp. 587–599. ISSN: 0022-3751 (cit. on p. 13).

[14] Tomoki Fukai and Shigeru Tanaka. «A Simple Neural Network Exhibiting Selective Activation of Neuronal Ensembles: From Winner-Take-All to Winners-Share-All». eng. In: *Neural computation* 9.1 (1997), pp. 77–97. ISSN: 1530-888X (cit. on pp. 14, 40).

[15] Shigeru Tanaka. «Theory of self-organization of cortical maps: Mathematical framework». eng. In: *Neural networks* 3.6 (1990), pp. 625–640. ISSN: 0893-6080 (cit. on p. 17).

[16] J. J. Hopfield. «Neural Networks and Physical Systems with Emergent Collective Computational Abilities». eng. In: *Proceedings of the National Academy of Sciences - PNAS* 79.8 (1982), pp. 2554–2558. ISSN: 0027-8424 (cit. on p. 19).

[17] Naoshige Uchida and Zachary F Mainen. «Speed and accuracy of olfactory discrimination in the rat». eng. In: *Nature neuroscience* 6.11 (2003), pp. 1224–1229. ISSN: 1097-6256 (cit. on p. 20).

[18] Lauren M. Jones, Alfredo Fontanini, Brian F. Sadacca, Paul Miller, and Donald B. Katz. «Natural Stimuli Evoke Dynamic Sequences of States in Sensory Cortical Ensembles». eng. In: *Proceedings of the National Academy of Sciences - PNAS* 104.47 (2007), pp. 18772–18777. ISSN: 0027-8424 (cit. on p. 20).

[19] Longnian Lin, Remus Osan, Shy Shoham, Wenjun Jin, Wenqi Zuo, Joe Z. Tsien, and Thomas C. Südhof. «Identification of Network-Level Coding Units for Real-Time Representation of Episodic Experiences in the Hippocampus». eng. In: *Proceedings of the National Academy of Sciences - PNAS* 102.17 (2005), pp. 6125–6130. ISSN: 0027-8424 (cit. on p. 20).

[20] Maxim Bazhenov, Mark Stopfer, Mikhail Rabinovich, Henry D.I Abarbanel, Terrence J Sejnowski, and Gilles Laurent. «Model of Cellular and Network Mechanisms for Odor-Evoked Temporal Patterning in the Locust Antennal Lobe». eng. In: *Neuron (Cambridge, Mass.)* 30.2 (2001), pp. 569–581. ISSN: 0896-6273 (cit. on p. 20).

[21] Gilles LAURENT, Mark STOPFER, Rainer W FRIEDRICH, Misha I RABINOVICH, Alexander VOLKOVSKII, and Henry DI ABARBANEL. «Odor encoding as an active, dynamical process : Experiments, computation, and theory». eng. In: *Annual review of neuroscience* 24.1 (2001), pp. 263–297. ISSN: 0147-006X (cit. on p. 20).

[22] M.I Rabinovich, R Huerta, A Volkovskii, H.D.I Abarbanel, M Stopfer, and G Laurent. «Dynamical coding of sensory information with competitive networks». eng. In: *Journal of physiology, Paris* 94.5 (2000), pp. 465–471. ISSN: 0928-4257 (cit. on p. 20).

[23] Valentin S Afraimovich, Mikhail I Rabinovich, and Pablo Varona. «Heteroclinic Contours in Neural Ensembles and the Winnerless Competition Principle». eng. In: *International journal of bifurcation and chaos in applied sciences and engineering* 14.4 (2004), pp. 1195–1208. ISSN: 0218-1274 (cit. on pp. 21, 27, 28, 30, 31, 34, 35, 58).

[24] Robert M May and Warren J Leonard. «Nonlinear Aspects of Competition Between Three Species». eng. In: *SIAM journal on applied mathematics* 29.2 (1975), pp. 243–253. ISSN: 1095-712X (cit. on pp. 21, 27, 59).

[25] Robert M. (Robert McCredie) May. *Stability and complexity in model ecosystems*. eng. Monographs in population biology ; 6. Princeton, N.J: Princeton University Press. ISBN: 0691081255 (cit. on pp. 22, 29).

[26] Chia-Wei Chi, Sze-Bi Hsu, and Lih-Ing Wu. «On the Asymmetric May-Leonard Model of Three Competing Species». eng. In: *SIAM journal on applied mathematics* 58.1 (1998), pp. 211–226. ISSN: 0036-1399 (cit. on p. 27).

[27] VALENTIN S AFRAIMOVICH, SZE-BI HSU, and HUEY-ER LIN. «CHAOTIC BEHAVIOR OF THREE COMPETING SPECIES OF MAY–LEONARD MODEL UNDER SMALL PERIODIC PERTURBATIONS». eng. In: *International journal of bifurcation and chaos in applied sciences and engineering* 11.2 (2001), pp. 435–447. ISSN: 0218-1274 (cit. on pp. 27, 34).

[28] M Rabinovich, A Volkovskii, P Lecanda, R Huerta, H D Abarbanel, and G Laurent. «Dynamical encoding by networks of competing neuron groups: winnerless competition». eng. In: *Physical review letters* 87.6 (2001), pp. 068102–681024. ISSN: 0031-9007 (cit. on pp. 27, 35).

[29] P. Shilnikov. «Methods of qualitative theory in nonlinear dynamics; part II». eng. In: *Scitech Book News* 26.3 (2002). ISSN: 0196-6006 (cit. on pp. 29, 30, 34).

[30] Valentin Afraimovich and Sze-Bi Hsu. *Lectures on chaotic dynamical systems*. AMS/IP studies in advanced mathematics. Providence, RI: American Mathematical Society, 2002. URL: `https://cds.cern.ch/record/2279761` (cit. on p. 34).

[31] A L Hodgkin and A F Huxley. «A quantitative description of membrane current and its application to conduction and excitation in nerve. 1952». eng. In: *Bulletin of mathematical biology* 52.1-2 (1990), 25–71, discussion 5–23. ISSN: 0092-8240 (cit. on pp. 37, 38).

[32] E.M Izhikevich. «Which model to use for cortical spiking neurons?» eng. In: *IEEE transactions on neural networks* 15.5 (2004), pp. 1063–1070. ISSN: 1045-9227 (cit. on p. 41).

[33] Olaf Sporns and Rolf Kötter. «Motifs in brain networks». eng. In: *PLoS biology* 2.11 (2004), e369–e369. ISSN: 1545-7885 (cit. on p. 41).

[34] Thomas Nowotny and Mikhail I Rabinovich. «Dynamical origin of independent spiking and bursting activity in neural microcircuits». eng. In: *Physical review letters* 98.12 (2007), pp. 128106–128106. ISSN: 0031-9007 (cit. on pp. 41, 43, 45, 46).

[35] W Rall, R E Burke, T G Smith, P G Nelson, and K Frank. «Dendritic location of synapses and possible mechanisms for the monosynaptic EPSP in motoneurons». eng. In: *Journal of neurophysiology* 30.5 (1967), pp. 1169–1193. ISSN: 0022-3077 (cit. on p. 42).

[36] Jonathan E Rubin. «Surprising Effects of Synaptic Excitation». eng. In: *Journal of computational neuroscience* 18.3 (2005), pp. 333–342. ISSN: 0929-5313 (cit. on p. 42).

[37] Philip Seliger, Lev S Tsimring, and Mikhail I Rabinovich. «Dynamics-based sequential memory: winnerless competition of patterns». eng. In: *Physical review. E, Statistical, nonlinear, and soft matter physics* 67.1 Pt 1 (2003), pp. 011905–011905. ISSN: 1539-3755 (cit. on pp. 47, 48).

[38] J O'Keefe and J Dostrovsky. «The hippocampus as a spatial map. Preliminary evidence from unit activity in the freely-moving rat». eng. In: *Brain research* 34.1 (1971), pp. 171–175. ISSN: 0006-8993 (cit. on p. 47).

[39] John O'Keefe. *The hippocampus as a cognitive map*. eng. Oxford: Clarendon Press, 1978. ISBN: 0198572069 (cit. on p. 47).

[40] Emma R Wood, Paul A Dudchenko, and Howard Eichenbaum. «The global record of memory in hippocampal neuronal activity». eng. In: *Nature (London)* 397.6720 (1999), pp. 613–616. ISSN: 0028-0836 (cit. on p. 48).

[41] H Eichenbaum, P Dudchenko, E Wood, M Shapiro, and H Tanila. «The hippocampus, memory, and place cells: is it spatial memory or a memory space?» eng. In: *Neuron (Cambridge, Mass.)* 23.2 (1999), pp. 209–226. ISSN: 0896-6273 (cit. on p. 48).

[42] D. O. (Donald Olding) Hebb. *The organization of behavior; : a neuropsychological theory.* eng. A Wiley book in clinical psychology. New York, Wiley, 1949 (cit. on p. 48).

[43] Bill Baird and Frank Eeckman. «A Normal Form Projection Algorithm for Associative Memory». In: *Associative Neural Memories: Theory and Implementation*. University Press, 1993, pp. 135–166 (cit. on p. 48).

[44] Esther D Gutiérrez and Juan Luis Cabrera. «A neural coding scheme reproducing foraging trajectories». eng. In: *Scientific reports* 5.1 (2015), pp. 18009–18009. ISSN: 2045-2322 (cit. on p. 52).

[45] Pablo Varona, Mikhail I Rabinovich, Allen I Selverston, and Yuri I Arshavsky. «Winnerless competition between sensory neurons generates chaos: A possible mechanism for molluscan hunting behavior». eng. In: *Chaos (Woodbury, N.Y.)* 12.3 (2002), pp. 672–677. ISSN: 1054-1500 (cit. on p. 53).

[46] M. W. Hirsch and Hal Smith. «Chapter 4 Monotone Dynamical Systems». English (US). In: *Handbook of Differential Equations*. Ed. by A. Canada, P. Drabek, and A. Fonda. Handbook of Differential Equations: Ordinary Differential Equations. 2006, pp. 239–357. ISBN: 9780444520272. DOI: 10.1016/S1874-5725(05)80006-9 (cit. on p. 56).

[47] S Smale. «On the differential equations of species in competition». eng. In: *Journal of mathematical biology* 3.1 (1976), pp. 5–7. ISSN: 1432-1416 (cit. on p. 56).

[48] Stephen Baigent. «Geometry of carrying simplices of 3-species competitive Lotka–Volterra systems». eng. In: *Nonlinearity* 26.4 (2013), pp. 1001–1029. ISSN: 1361-6544 (cit. on p. 57).

[49] M W Hirsch. «Systems of differential equations which are competitive or cooperative: III. Competing species». eng. In: *Nonlinearity* 1.1 (1988), pp. 51–71. ISSN: 1361-6544 (cit. on p. 57).